The Stress of a Serve

Biomechanical Quantification of Shoulder Muscle Load in the Tennis Serve

Eric Verdoes

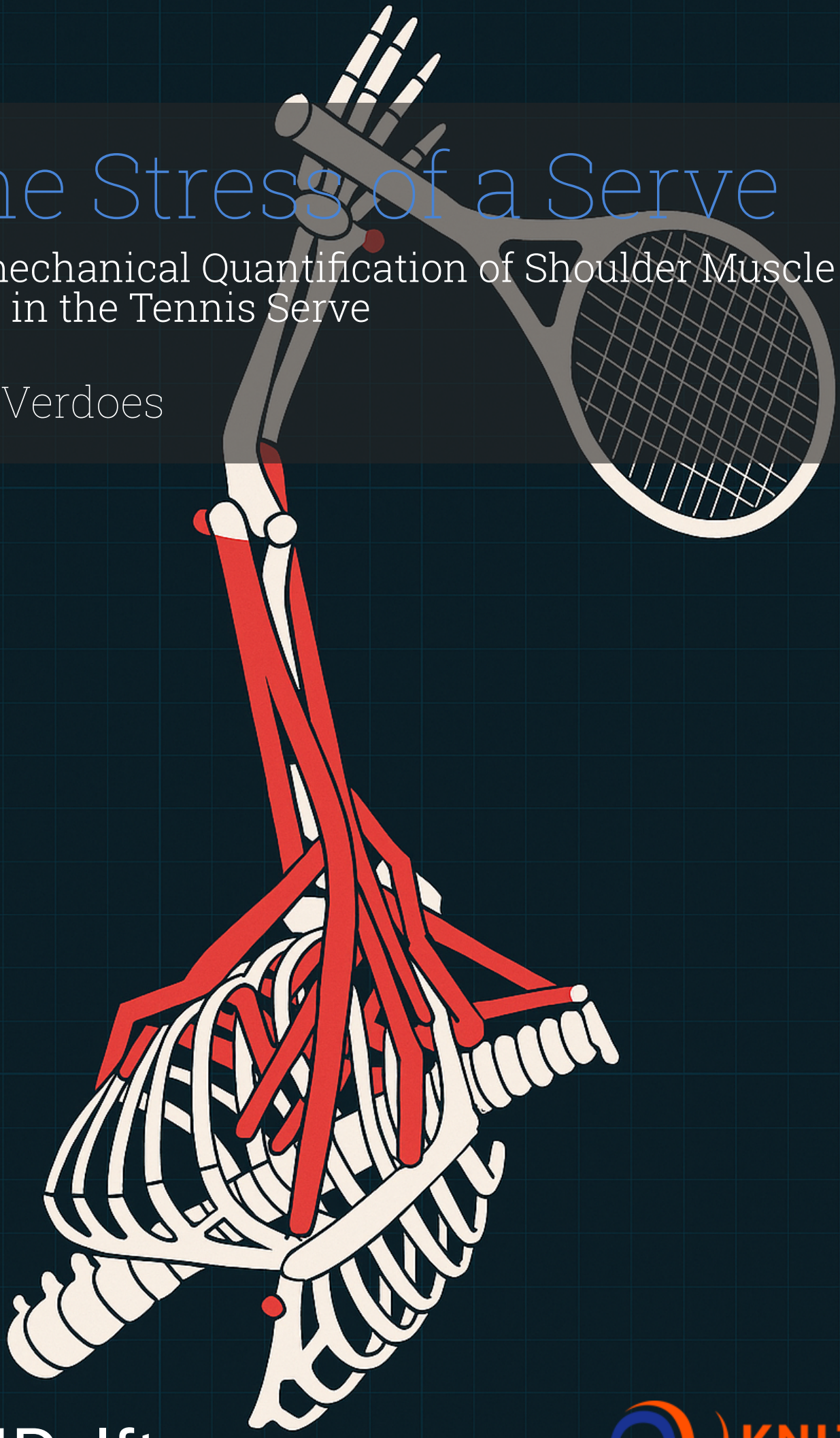

Delft University of Technology

TU Delft

KNLTB

The Stress of a Serve

Biomechanical Quantification of Shoulder Muscle Load in the Tennis Serve

by

Eric Verdoes

Supervisors:	Ajay Seth, Aldo Hoekstra
Project Duration:	December 2024 - December 2025
Faculty:	Faculty of Mechanical Engineering, Delft

TU Delft KNLTB

Preface

This thesis marks the final step in my graduation project, carried out in collaboration between the KNLTB and TU Delft. Throughout this work, I have had the opportunity to explore the biomechanics of the tennis serve and contribute to ongoing research within a professional sports environment. Working on this thesis pushed me both technically and conceptually, and I learned a great deal through the setback and progress along the way.

I would like to express my sincere gratitude to my supervisors, Ajay Seth (TU Delft) and Aldo Hoekstra (KNLTB), for giving me the opportunity to conduct this research and for their continuous guidance, support, and constructive feedback throughout the project. Their guidance directly influenced the direction of this work and helped me develop confidence in my own reasoning and decision-making during the project. I am also thankful to my colleagues at the KNLTB for the welcoming atmosphere and daily collaboration that made working there both productive and enjoyable.

Eric Verdoes
Delft, December 2025

Summary

Shoulder injuries are common in tennis and are often associated with the high joint loads generated during the serve. While previous work has described kinematics, joint kinetics, and energy transfer along the kinetic chain, less is known about how individual shoulder muscles generate, transfer and absorb mechanical energy during the serve. The aim of this thesis was to investigate how mechanical energy is generated, transferred, and absorbed in the upper extremity during the tennis serve, with a specific focus on the shoulder and elbow joints and the muscle groups responsible for accelerating and decelerating the arm.

Data from five male competitive tennis players were analysed. Three-dimensional motion capture and surface EMG were combined with an upper-extremity OpenSim model that included the thorax, shoulder complex, elbow, forearm, and racket. Inverse kinematics and inverse dynamics were used to obtain joint kinematics and net joint moments. Static optimization (SO) was then applied to solve for muscle forces that generated the experimental accelerations. Muscle power and work were computed for all shoulder muscles, and generalized actuator work was quantified to assess the contribution of non-muscular actuators. The serve was divided into three time windows based on kinetic energy peaks of the thorax and forearm: (1) trophy position to thorax peak, (2) thorax peak to forearm peak, and (3) forearm peak to maximum internal rotation (MIR).

Model verification showed acceptable marker tracking accuracy for most markers, with distal marker RMSE values predominantly below 10 mm and proximal markers generally below 20 mm. Reserve actuator work remained small in most coordinates and time windows, but increased around ball impact for shoulder axial rotation and elbow flexion. EMG–SO comparisons demonstrated moderate-to-strong agreement for the pectoralis major and more variable correlations for the triceps, latissimus dorsi, deltoid, and biceps, reflecting both modelling assumptions and physiological factors.

During the early and mid-acceleration phase (trophy position—where the player tosses the ball while preparing to serve, standing as if holding a trophy—to forearm peak), the shoulder–elbow joint system showed relatively small changes in net joint work, while substantial positive and negative muscle work occurred simultaneously across muscles. The Serratus Anterior, Subscapularis, and medial deltoid consistently produced positive work, whereas the infraspinatus, teres minor, rhomboids, and parts of the trapezius absorbed energy. These patterns suggest that many muscles acted less as pure rotators and more as stabilisers within the “compressor cuff” and scapular control system, helping to manage trunk-to-arm energy transfer rather than simply increasing total system energy.

In the late phase (forearm peak to MIR), all participants showed large negative joint work, consistent with rapid arm deceleration. Muscle absorption during this phase was distributed across scapular stabilisers, abductors, horizontal abductors, and (to a lesser extent) the posterior rotator cuff. The medial deltoid and lower trapezius frequently exhibited large negative work values, indicating a prominent role in decelerating the elevated arm and stabilising the scapula. Functional grouping of muscles revealed clear inter-individual differences: some players showed a broad distribution of absorption across all groups, whereas others showed scapular-dominant or abductor-dominant strategies.

Overall, this thesis demonstrates that the tennis serve is characterised by patterns of muscle-level energy generation, transfer, and absorption that are not visible from net joint work alone. The results highlight the importance of scapular muscles working eccentrically to maintain scapular control (e.g., Rhomboids and Lower Trapezius), as well as shoulder abductors, alongside the posterior cuff, in managing deceleration loads at the shoulder. The work also illustrates how musculoskeletal modelling can be used to link kinetic-chain mechanics with individual muscle contributions, while emphasising the need for improved scapular modelling, subject-specific anatomy, and the inclusion of external forces in future studies.

Contents

Nomenclature

Abbreviations

Abbreviation	Definition
DOF	Degree of Freedom
EMG	Electromyography
ID	Inverse Dynamics
IK	Inverse Kinematics
KNLTB	Dutch Tennis Federation
ROM	Range Of Motion
SO	Static Optimization

Symbols

Symbol	Definition	Unit
a	Acceleration	[m/s^2]
a_m	Muscle activation level	[-]
C	Coriolis and Centrifugal force	[N]
e_m	Marker error	[m]
e_q	Coordinate error	[$^\circ$]
F	Force	[N]
F_m^0	Maximum isometric force	[N]
G	Gravitational force	[N]
J	Objective function	[-]
l_m	Muscle fiber velocity	[m/s]
m	Mass	[kg]
M	Mass inertia matrix	[kg]
N	Number	[-]
P	Power	[W]
p	Marker position	[m]
q	Coordinate angle	[rad]
$\dot{q}$	Coordinate angular velocity	[rad/s]
$\ddot{q}$	Coordinate angular acceleration	[rad/s^2]
$r_{m,j}$	Moment arm of muscle m about joint j	[m]
s	Scale factor	[-]
t	Time	[s]
W	Work	[J]
w	Marker weight factor	[-]
$\dot{\theta}$	Coordinate angular velocity	[rad/s]
$\ddot{\theta}$	Coordinate angular acceleration	[rad/s^2]
τ	Torque vector	[N]

1

Introduction

Tennis is a globally popular sport played by millions of people across different ages and skill levels. In the Netherlands alone, the Dutch Tennis Federation has over 844,000 registered members [7]. Tennis players are exposed to repetitive high-intensity strokes that generate substantial joint loads. Shoulder injuries are among the most frequent overuse injuries in tennis, often leading to reduced performance or time lost from competition. Identifying the mechanical contributions to these injuries can help refine both prevention and rehabilitation approaches in practice.

1.1. Breakdown of the serve

The tennis serve accounts for approximately 45–60% of all strokes performed during a match and is among the most complex and physically demanding movements in the sport. The advantage it provides is reflected in performance statistics: top male players win over 80% of points following their first serve, while the best female players exceed 70% [16].

Mechanically, the serve functions as a multibody system where energy and angular momentum are transferred along the kinetic chain from the lower limbs through the trunk, to the upper extremities and eventually the racket. This sequential energy transfer enables high racket-head velocities at ball impact, which are essential for serve effectiveness.

Although the movement is traditionally divided into eight phases [8], Figure 1.1 illustrates five key stages relevant to this study: release, loading, cocking, acceleration, and deceleration. The cocking, acceleration, and deceleration phases are of particular interest, as they involve the greatest shoulder joint loading and are most relevant to injury mechanisms. The start, ball impact, and finish phases are omitted here, as their biomechanical contribution is limited within the scope of this research.

1.2. The Kinetic Chain

The tennis serve is a complex whole–body movement in which force and motion are generated and transmitted through a coordinated sequence of body segments, commonly referred to as the *kinetic chain*. In effective serving, force originates in the lower limbs and is transferred through the pelvis and trunk before reaching the upper arm, forearm, hand, and racket. Classical biomechanical descriptions show that more than half of the kinetic energy delivered to the racket originates in the legs and trunk, underlining their importance in proximal force generation [8]. Mechanically, the kinetic chain functions through coordinated energy generation, transfer, and absorption across successive segments. High-quality energy flow from trunk to upper limb has been shown to increase ball speed while reducing loading at the shoulder and elbow, whereas disrupted energy flow requires compensatory actions at the upper limb and increases joint stresses [14].

The kinetic chain can also be described through the transfer of angular momentum between successive body segments. Angular momentum is defined as $L = I\omega$, where I is the moment of inertia and ω the segment's angular velocity. The moment of inertia represents the resistance of a segment to angular

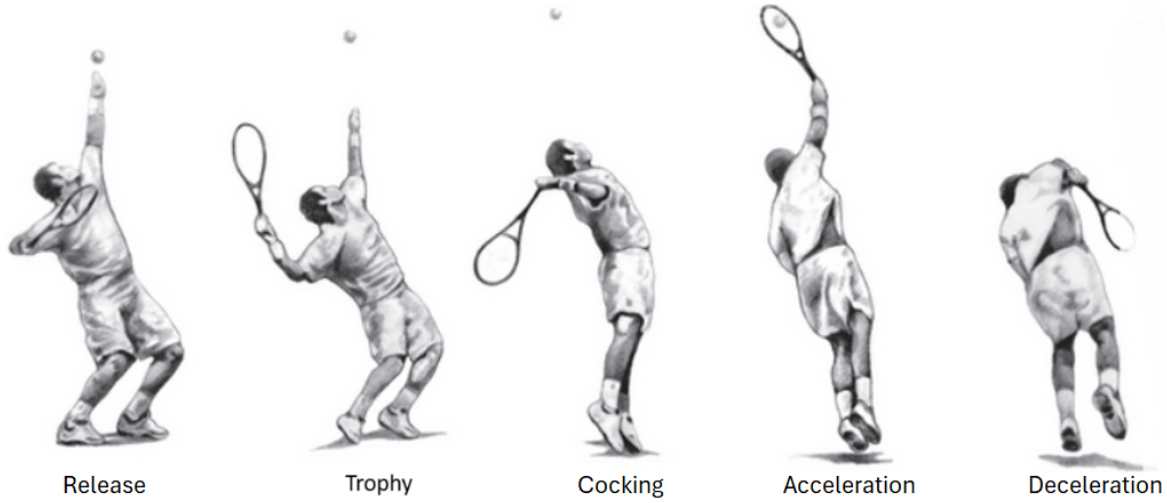

Figure 1.1: Phases of the tennis serve

acceleration and depends not only on its mass but also on how that mass is distributed relative to the axis of rotation. Proximal segments such as the pelvis and trunk have a large moment of inertia due to their greater mass and wider mass distribution, and can therefore generate substantial angular momentum even at relatively modest angular velocities. When this angular momentum is transferred to distal segments with progressively smaller moments of inertia—such as the upper arm, forearm, and finally the racket—the angular velocity must increase to conserve angular momentum. As a result, distal segments accelerate rapidly, producing the high racket-head speeds required for an effective serve. This mechanism corresponds to the classical summation-of-speed principle and underlies the proximal-to-distal sequencing characteristic of high-performance overhead motions [26].

Recent developments in tennis biomechanics have provided new insights into this coordination. Using inertial measurement units (IMUs), van Trigt and colleagues showed that professional tennis players do not always follow a strictly timed proximal-to-distal sequence, and instead the magnitude of angular velocities—particularly of the trunk and upper arm—is the strongest contributor to ball speed [26]. Additional work highlights how subtle intersegmental timing differences, often not observable visually, influence the efficiency of energy and angular momentum transfer through the kinetic chain [25]. Broader sport-science perspectives indicate that disruptions in the kinetic chain can increase mechanical loads on the medial elbow and shoulder in overhead athletes [24].

Technical deviations during the serve also reveal the sensitivity of joint loading to kinetic chain mechanics. Inefficient movement patterns–such as prolonged horizontal abduction, insufficient leg drive, or altered trunk rotation—lead to elevated internal rotation torque at the shoulder and increased varus torque at the elbow, without necessarily improving performance [13]. These patterns illustrate how altered sequencing or segmental contributions disrupt the normal transfer of energy and angular momentum.

1.2.1. Insights from Baseball Pitching

Comparable mechanisms are evident in baseball pitching, where the kinetic chain and angular momentum transfer principles are similarly critical. Manzi et al. demonstrated that trunk flexion, horizontal shoulder positioning, and timing of maximum external rotation are key predictors of anterior shoulder force in pitchers [12]. Further analyses showed that excessive horizontal adduction increases shoulder distraction forces, while excessive horizontal abduction disrupts torque patterns and reduces performance [10]. Yanai et al. identified that poor coordination between scapular and humeral motion can lead to hyperangulation, a configuration linked to internal impingement risk [29]. In addition, baseball pitches executed with ideal proximal-to-distal sequencing were found to achieve higher ball velocities without increasing shoulder or elbow loading, whereas disrupted sequencing necessitated compensatory upper-limb actions that increased joint forces [11].

Across both tennis and baseball, these findings consistently show that efficient kinetic chain function and coherent angular momentum transfer minimize upper-limb loading, while disruptions in sequencing or proximal contribution increase mechanical demands on the shoulder and elbow. These principles provide a foundational biomechanical framework for understanding upper-limb joint loading in high-performance tennis.

1.3. Musculoskeletal modeling

While the available biomechanical research provides useful insights into movement patterns, joint forces and energy flows [8, 15], it does not fully connect those findings to what is happening at the tissue level. That is where musculoskeletal modeling could be a big step forward [22]. It allows for simulations of internal forces, like muscle loading during critical points in the serve. This is especially interesting during the acceleration and deceleration (or follow-though) phases, which are often linked to shoulder injuries to the rotator cuff tears or scapular dyskinesis [28, 17] By using motion capture data together with individualized musculoskeletal models, researchers can better estimate how specific rotator cuff and scapular muscles contribute during different phases of the serve. This approach gives a better insight of how certain joint angles or torque levels might lead to increased stress on the rotator cuff tendons or around the scapula.

Understanding muscle contributions in relation to the kinetic chain can clarify how muscle mechanics influence shoulder loads.

1.4. Research Goal

The goal of this thesis is to investigate how mechanical energy is generated, transferred, and absorbed across the shoulder complex. Rather than estimating absolute joint loading magnitudes, the study aimed to quantify the relative mechanical roles of the shoulder and elbow joints, and to identify the muscle groups primarily responsible for accelerating and decelerating the arm and racket.

This motivated the following research questions:

1. **Energy Transfer Across the Kinetic Chain:** How is mechanical energy transferred from the trunk through the shoulder, and elbow joints during the tennis serve?
2. **Muscle Contributions to Acceleration and Deceleration:** Which muscle groups contribute most to the transfer of mechanical energy during the acceleration phase, and which muscle groups are responsible for absorbing energy during the deceleration phase?

2

Method

2.1. Data Collection

The data from a previous master thesis is used for this experiment [1]. This master thesis investigated the relationship between shoulder kinematics and pectoralis major muscle activity during the tennis serve in order to explore the potential role of hyperangulation in internal impingement syndrome in overhead athletes.

Eligible participants were required to have at least Level 5 ranking according to the KNLTB classification. In addition, participants could not have experienced any shoulder injury or shoulder pain in the three months prior to the study. Fourteen male tennis players meeting these criteria took part in this experimental laboratory study, each performing 10 first serves and 10 second serves. For the current study, the data of the 10 first serves of 5 participants is used. In this thesis, the data of the 10 first serves of 5 participants were used.

Three-dimensional marker data from nineteen reflective markers were recorded with twelve motion capture cameras (OptiTrack Flex 13, OptiTrack™, Corvalis, United States) at 120 Hz. Before each participant's measurements, the system was calibrated to define camera position, orientation, and a global coordinate system (XG: left, YG: upward, ZG: forward from baseline to net). Table 2.1b shows which marker positions are utilized and which muscles are tracked. Note that Figure 2.1a includes markers on the pelvis (11-14) and hand (10), which were not incorporated in the model. Electromyography (EMG) signals were recorded from the Pectoralis Major (clavicular and sternal heads), Latissimus Dorsi, Triceps (medial head), and Biceps (short head) with a bipolar electrode configuration, using the biosignalsplux Researcher kit (biosignalsplux, Lisboa, Portugal) at a sampling frequency of 2000 Hz.

2.2. Data Processing

To enable a fair comparison between the simulated muscle activations from Static Optimization (SO) and the experimentally measured EMG signals, both datasets were aligned, cropped, and normalized to the duration of each serve.

First, each serve trial was cropped based on characteristic kinematic events detected from the thorax motion. Specifically, the local maxima (Windup) and minima (Finish) of the thorax vertical translation (T_y) were used to define the start and end of the motion cycle, shown in 2.2. Additionally, the horizontal acceleration of the thorax in the x-direction (T_x), obtained by differentiating twice, was used to identify the frame corresponding to the peak forward acceleration of the trunk. These key moments ensured consistent serve segmentation across trials.

The biosignalsplux device also included a built-in accelerometer located at the sternum, providing an x-directed acceleration signal. This signal was used to synchronize the EMG data with the kinematic recordings by matching the timing of the peak horizontal acceleration to that of the corresponding T_x peak from the motion capture data.

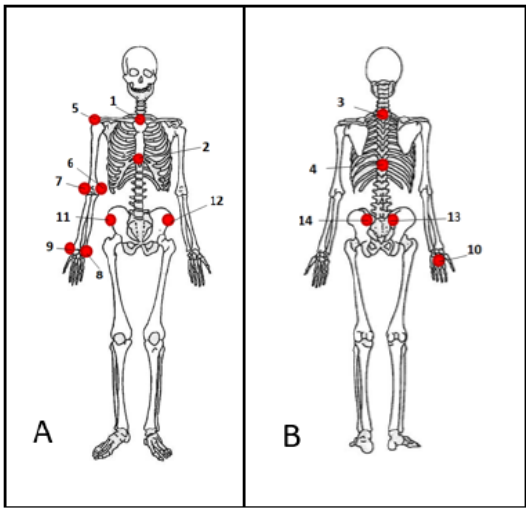

(a) Marker placement overview.

No.	Marker location	Segment
1	Incisura jugularis	Thorax
2	Xyphoid process	Thorax
3	7th cervical vertebra	Thorax
4	10th thoracic vertebra	Thorax
5	Acromion	Upper arm
6	Medial epicondyle of humerus	Upper arm
7	Lateral epicondyle of humerus	Upper arm
8	Ulnar styloid process	Hand
9	Radial styloid process	Hand

(b) Marker locations and associated body segments.

Figure 2.1: Marker setup and corresponding marker locations.

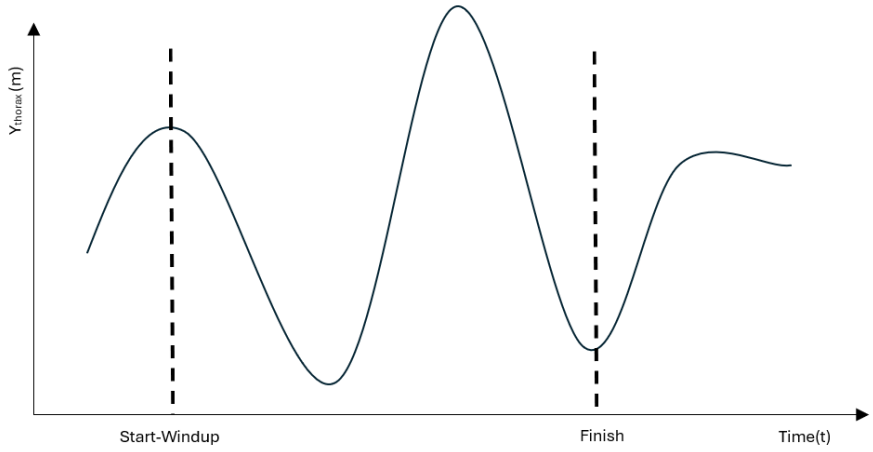

Figure 2.2: Visualization of the serve cropping points from Windup to Finish

After synchronization, the minimum frame count among all cropped IK files was used to resample both the EMG and SO activation data to a uniform length, ensuring consistency across serves. The resampled data were then time-normalized to a 0 to 100% motion cycle representation of the serve, enabling a point-by-point comparison between the EMG and simulated activation profiles.

Finally, the Pearson correlation coefficient was computed between each EMG signal and its corresponding SO activation to evaluate the similarity in activation timing and shape across the normalized serve cycle

2.3. OpenSim Model

An OpenSim shoulder model (Figure 2.1) was used in this study [21]. The full model consists of 8 bodies, 17 degrees of freedom (DOFs), and 35 muscles. It includes the thorax, right arm, and racket, with muscles modeled around the shoulder complex only. The spine is represented as a single rigid segment, which may introduce errors in torso motion. Similarly, the wrist joint is not modeled, resulting in the forearm, hand and racket being treated as a single rigid element without muscles.

2.3.1. Model Changes

One modification was made to the range of motion (ROM) of the humeral axial rotation coordinate. In the original model, axial rotation was limited to –90°, whereas advanced or higher level tennis players can exceed 150° of external rotation during the serve. Therefore, the ROM was extended to –160°. Due to time constraints, a complete validation of the updated model could not be performed. Therefore, it was assumed that the model was suitable for the intended analyses if the moment arms of the three subscapularis muscle paths (i.e. superior, medial, inferior) remained positive and continuous throughout internal rotation.

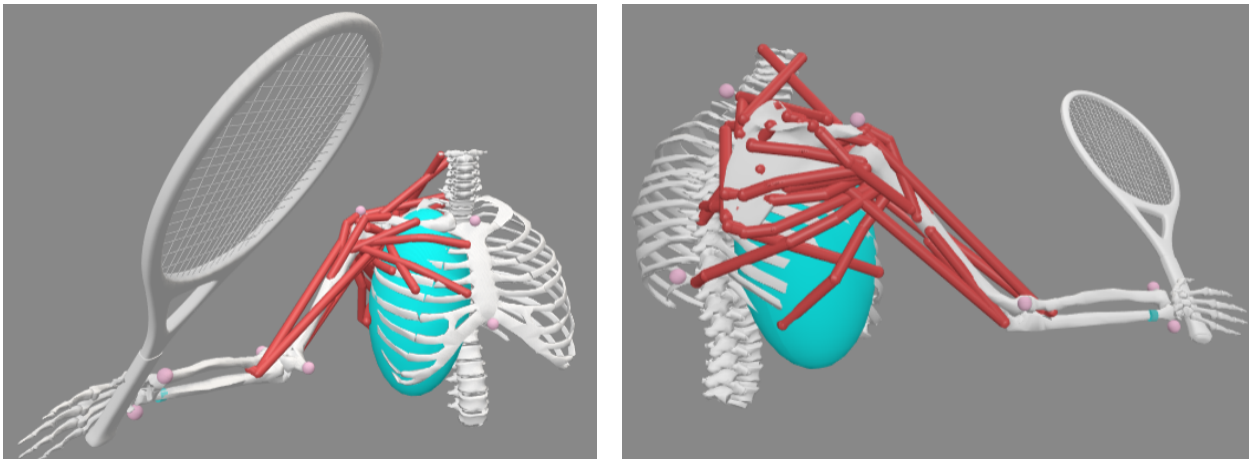

(a) Front view **(b)** Back view

Figure 2.3: OpenSim model shown from front and back perspectives.

In addition, a right hand and tennis racket were added to the model. Although marker data for these segments were not analyzed in the present study, they were included because their mass and inertia contribute to the loading on the shoulder.

2.4. Scaling

Before performing inverse kinematics, the model must be scaled to match the dimensions of the participant. In OpenSim, scaling is performed using linear factors for the x, y, and z directions of each segment. These scale factors are computed from the relative distances between pairs of markers in the model and the corresponding distances in the experimental data. The general formula is:

$$s = \frac{\|\mathbf{p}_{m,i} - \mathbf{p}_{m,j}\|}{\|\mathbf{p}_{e,i} - \mathbf{p}_{e,j}\|} \tag{2.1}$$

where $\mathbf{p}_{m,i}$ and $\mathbf{p}_{m,j}$ are the positions of model markers i and j, and $\mathbf{p}_{e,i}$ and $\mathbf{p}_{e,j}$ are the corresponding experimental marker positions. After scaling, the positions of the model markers are adjusted to match the experimental marker data as closely as possible, ensuring that the virtual model represents the participant's anthropometry.

2.5. Inverse Kinematics

In OpenSim's inverse kinematics (IK) tool, the model's joint coordinates are estimated by solving an optimization problem at every time frame. The objective is to reduce the mismatch between the experimental data and the model by minimizing two types of errors within a weighted least-squares framework (Equation 2.2).

Marker error (e_m): the spatial distance between a model marker (calculated from the estimated coordinates) and its corresponding experimental marker (Equation 2.3).

Coordinate error (e_q): the difference between a measured joint coordinate value q_{exp} and the value computed from the model q (Equation 2.4).

By assigning different weights to markers and coordinates, the user can specify which data points should have greater influence in the optimization. This makes it possible, for example, to prioritize certain anatomical landmarks or joint angles when fitting the model to motion capture data. In this simulation, higher marker weights were given to more distal markers, and coordinate weight were given to the scapula coordinates to ensure acceptable marker tracking and physiological reasonable motion of the scapula.

$$\min \left(\sum_{i=1}^{n_m} w_i \, e_{m,i}^2 + \sum_{j=1}^{n_q} w_j \, e_{q,j}^2 \right) \tag{2.2}$$

$$e_{m,i} = \mathbf{p}_{\text{exp},i} - \mathbf{p}_i(\mathbf{q}) \tag{2.3}$$

$$e_{q,j} = q_{\text{exp},j} - q_j \tag{2.4}$$

The result of the inverse kinematics step is a time series of joint coordinate values that align the model with the experimental marker data as closely as possible. To evaluate how well the model reproduces the motion, marker errors are examined for each marker across all recorded trials.

2.6. Inverse Dynamics

The inverse dynamics (ID) tool estimates the generalized forces, such as joint moments and reaction forces, that are required to reproduce a specific motion. This analysis uses the kinematic data obtained from the IK step as input. Because no external forces were measured in this study, external load data are excluded from the ID computations.

In essence, the inverse dynamics process solves the relationship between mass, acceleration, and force, expressed as $\mathbf{F} = m\mathbf{a}$, by applying the equations of motion to the model.

The general dynamic equation of motion can be formulated as:

$$\mathbf{M}(\mathbf{q})\,\ddot{\mathbf{q}} + \mathbf{C}(\mathbf{q}, \dot{\mathbf{q}}) + \mathbf{G}(\mathbf{q}) = \boldsymbol{\tau} \tag{2.5}$$

where:

- N denotes the number of degrees of freedom,
- $\mathbf{q}, \dot{\mathbf{q}}, \ddot{\mathbf{q}} \in \mathbb{R}^N$ represent the generalized position, velocity, and acceleration vectors,
- $\mathbf{M}(\mathbf{q}) \in \mathbb{R}^{N \times N}$ is the mass (inertia) matrix of the system,
- $\mathbf{C}(\mathbf{q}, \dot{\mathbf{q}}) \in \mathbb{R}^N$ corresponds to the Coriolis and centrifugal force vector,
- $\mathbf{G}(\mathbf{q}) \in \mathbb{R}^N$ is the gravitational force vector, and
- $\boldsymbol{\tau} \in \mathbb{R}^N$ represents the vector of generalized torques.

Given that the kinematics of the model are known from the motion capture data and via IK, all terms on the left-hand side of Equation 2.5 are determined. The only unknown term is the generalized force vector $\boldsymbol{\tau}$. The inverse dynamics procedure therefore uses the known motion of the model to compute these forces, effectively estimating the joint torques necessary to produce the observed movement. These results of the ID will later be used to validate the model.

2.7. Static Optimization

To estimate individual muscle forces during the tennis serve, a SO analysis was performed in OpenSim. Static Optimization extends inverse dynamics by resolving the net joint moments, obtained from ID, into the contributions of individual muscles at each instant in time. The kinematic results from the IK analysis, low-pass filtered at 6 Hz, were used as input to compute the corresponding muscle forces that generate the observed joint moments.

The Static Optimization problem is formulated as a frame-by-frame optimization, where muscle activations are estimated by minimizing a cost function that represents the total muscular effort (Equation 2.6). The optimization seeks the set of activations that best reproduce the joint moments obtained from ID, while accounting for each muscle's force-length-velocity properties through the equilibrium constraints (Equation 2.7).

$$J = \sum_{m=1}^{n} (a_m)^p \tag{2.6}$$

$$\sum_{m=1}^{n} \left[a_m \, f\left(F_m^0, l_m, v_m\right) \right] r_{m,j} = \tau_j \tag{2.7}$$

where

- a_m is the activation level of muscle m,
- F_m^0 is its maximum isometric force,
- l_m and v_m are the muscle fiber length and velocity, respectively,
- $f(F_m^0, l_m, v_m)$ represents the muscle's force–length–velocity surface,
- $r_{m,j}$ is the moment arm of muscle m about joint axis j,
- τ_j is the net joint torque about joint axis j,
- n is the total number of muscles in the model, and
- p is a user-defined constant (commonly $p = 2$) determining the weighting of activations in the cost function.

The resulting muscle activations are then used to compute the corresponding muscle forces, assuming an rigid tendon and excluding contributions from passive muscle elements. This assumption implies that activation dynamics and tendon compliance are neglected. The output SO output consists of time-varying muscle activations and forces.

2.8. Verification and Validation

Verification and validation procedures were performed to assess the numerical correctness and physiological plausibility of the musculoskeletal model. Verification ensures that the implemented model correctly reproduces the measured kinematics, while validation evaluates whether the resulting dynamic quantities and muscle forces are physically meaningful.

2.8.1. Inverse Kinematics Verification

To evaluate how well the model reproduces the measured motion, marker errors were examined for each marker across all recorded trials. The root mean squared error (RMSE) between the experimental marker trajectories and the model's virtual markers was computed as an indicator of kinematic accuracy. Typical RMSE values reported for validated OpenSim models range between 10 mm and 20 mm for upper-limb markers, depending on model complexity and soft tissue artifact [23, 18, 19]. In this study, an RMSE below 10 mm for distal markers (e.g., wrist and elbow) and below 20 mm for proximal or trunk markers was considered acceptable. Lower RMSE values indicate a better match between experimental and simulated motion, and thus improved kinematic fidelity.

2.8.2. Model validation

To validate the model, the reserve actuator results from the SO analysis were compared to the ID results. In SO, reserve actuators are required to ensure dynamic consistency between the model and the experimental data. However, their contribution should be small enough to avoid influencing the interpretation of muscle forces and joint moments.

Following the recommended guidelines for OpenSim model validation [2], the contribution of the reserve actuators was evaluated by quantifying their mechanical work. The absolute mechanical work (both

eccentric and concentric) performed by each reserve actuator (W_j) was calculated for both the ID and SO results. This allowed assessment of whether the reserves contributed minimally to joint actuation, indicating that the primary joint torques were generated by the musculature rather than by reserve actuators. The mechanical work was computed as:

$$W_j = \int \tau_j \, \dot{\theta}_j \, dt \tag{2.8}$$

where τ_j is the actuator torque about joint axis j, and $\dot{\theta}_j$ is the corresponding joint angular velocity. The percentage of work performed by the SO reserve actuators relative to the total actuator work from ID was then determined to quantify their overall contribution to the motion. This step provides should show that reserve actuators were only minimally involved in reproducing the observed motion.

2.8.3. EMG Validation of Muscle Activations

To evaluate the physiological plausibility of the simulated muscle activations obtained from the SO analysis, the model results were compared with the experimentally measured surface EMG signals. This comparison assesses whether the model reproduces realistic patterns of muscle recruitment during the tennis serve.

The processed and time-normalized EMG signals were correlated with their corresponding SO-predicted muscle activations using the Pearson correlation coefficient (r), which quantifies the linear similarity between the two activation profiles:

$$r = \frac{\sum_{i=1}^{N}(x_i - \bar{x})(y_i - \bar{y})}{\sqrt{\sum_{i=1}^{N}(x_i - \bar{x})^2 \sum_{i=1}^{N}(y_i - \bar{y})^2}} \tag{2.9}$$

where x_i and y_i represent the normalized activation values from EMG and SO, respectively, $\bar{x}$ and $\bar{y}$ are their mean values, and N is the number of samples within the serve cycle. A higher correlation coefficient indicates greater agreement in the temporal pattern of activation between the experimental and simulated signals.

To account for the electromechanical delay present in EMG signals, a lag-corrected correlation ($r_{\max}$) was computed. Correlations were evaluated across a window of -10 frames (approximately -83 ms at 120 Hz), and the maximum correlation value and corresponding lag were selected. This procedure compensates for physiological activation-to-force delays, allowing a fair comparison between the EMG signals and the activation results from SO.

Correlation coefficients were computed for each muscle and serve, and both the unlagged (r) and lag-corrected ($r_{\max}$) values were summarized across participants. The strength of the correlations was interpreted as: weak ($r < 0.3$), moderate ($0.3 \leq r < 0.5$), and strong ($r \geq 0.5$). Strong or improved $r_{\max}$ values indicate that the model captured the timing and shape of muscle activation with good physiological consistency.

2.9. Mechanical Work and Energy Transfer Analysis

To quantify how individual muscles contribute to the transfer of angular momentum during the tennis serve, a full decomposition of segmental and muscular work was performed using inverse and muscle dynamics. All analyses were performed across the windows defined by classical event timestamps (trophy, MER, MOI, MIR) and kinematic energy peaks of the thorax, humerus and forearm.

2.9.1. Energy Balance

The total mechanical energy of the system during the serve can be defined as the sum of the potential and kinetic energies of all body segments. The potential energy is defined as the sum of the segment-specific potential energies:

$$E_{\text{pot}} = \sum_i m_i g h_i,$$

where m_i and h_i denote the mass and vertical position of segment i, respectively.

Similarly, the kinetic energy is expressed as the sum of the translational and rotational kinetic energies of each segment:

$$E_{\text{kin}} = \sum_i \left(\frac{1}{2} m_i v_i^2 + \frac{1}{2} I_i \omega_i^2 \right),$$

where v_i is the linear velocity, I_i the segmental moment of inertia, and ω_i the angular velocity of segment i.

If no potential or kinetic energy is generated or absorbed by the muscles, the total energy of the system should remain approximately constant between take-off and landing. The only external energy loss during the motion is the energy dissipated during ball impact.

The resulting total energy balance is therefore

$$\Delta E_{\text{tot}}(t) = \Delta E_{\text{pot}}(t) + \Delta E_{\text{kin}}(t) + \Delta W_{\text{muscle}} - \Delta E_{\text{ball impact}}.$$

2.9.2. Muscle Power and Work

To determine how the change in total mechanical energy is produced or absorbed within the system, it is necessary to quantify the contribution of the individual upper-extremity muscles to joint power and joint work. This requires computing the muscle-induced power and work for each modeled muscle. Muscle fibre lengths for upper-extremity shoulder complex muscles were obtained from OpenSim's MuscleAnalysis tool, while muscle forces were extracted from the static optimization results. Together, these inputs allow computation of the muscle-specific mechanical work that contributes to the overall joint power and energy changes observed during the serve.

For each muscle m, fibre velocity $\dot{L}_m(t)$ was computed as the numerical time derivative of the fibre length $L_m(t)$. Muscle mechanical power was then computed as

$$P_m(t) = -F_m(t)\, \dot{L}_m(t), \tag{2.10}$$

where $F_m(t)$ is the muscle force. The sign convention ensures that:

- $P_m(t) > 0$: muscle performs positive work on the skeleton (concentric shortening),
- $P_m(t) < 0$: muscle performs negative (absorbs) on the skeleton (eccentric lengthening).

To obtain muscle work within each time window $[t_0, t_1]$, muscle power was integrated numerically:

$$W_m = \int_{t_0}^{t_1} P_m(t)\, dt. \tag{2.11}$$

2.9.3. Generalized Actuator Power and Work

OpenSim static optimization reports the force produced by each generalized coordinate actuator. These actuator forces represent non-muscular contributions required to satisfy the equations of motion, such as contributions compensating for missing musculature or modelling simplifications.

Actuator mechanical power was computed for each actuator a as:

$$P_a(t) = Q_a(t)\, \dot{q}_a(t), \tag{2.12}$$

where $Q_a(t)$ is the actuator generalized torque and $\dot{q}_a(t)$ is the corresponding generalized speed from the kinematics analysis.

Actuators were further subdivided into:

- thorax actuators,
- shoulder actuators,
- elbow flexion/extension actuators,
- forearm pronation/supination actuators.

Reserve actuator work was decomposed as:

$$W_{\text{thorax}} = \sum_{i \in \text{thorax}} W_i, \tag{2.13}$$

$$W_{\text{shoulder}} = \sum_{i \in \text{shoulder}} W_i, \tag{2.14}$$

$$W_{\text{elbow}} = \sum_{i \in \text{elbow}} W_i, \tag{2.15}$$

$$W_{\text{forearm}} = \sum_{i \in \text{forarm}} W_i. \tag{2.16}$$

These quantities represent the net mechanical energy induced/absorbed by reserve actuators across the upper-extremity joints. This separation allowed quantification of how much of the net work at the shoulder and elbow joint were compensated by actuators.

For each time window, the following contributions were computed for:

- $W_{\text{ID, thorax}}, W_{\text{ID, shoulder}}, W_{\text{ID, elbow}}$,
- $W_{\text{act, shoulder}}, W_{\text{act, elbowflexion}}, W_{\text{act, prosup}}$,
- W_{m}

This allowed identification of whether, and which, joints required actuator support relative to the total work in that time window.

Averaging Across Serves

All quantities were computed for each serve individually. Mean and standard deviation across serves per participant were computed for each time window and used to generate both the bar plots (muscle- and actuator-specific work) and the segmental pie charts.

3

Results

3.1. Model Verification and Validation

3.1.1. Inverse Kinematics Verification

Figure 3.1 presents the marker tracking errors obtained from the inverse kinematics (IK) procedure, expressed as root mean squared error (RMSE) between the model marker locations and the experimentally recorded marker trajectories. The wrist markers shows RMSE values below 10 mm across all participants. The elbow markers show slightly larger variability, with RMSE values ranging from 6.2 mm to 15.8 mm. For the proximal markers, most RMSE values 14 out of 20 markers remain below 20 mm, while 6 out of 20 markers showed slightly larger errors ranging from 20.6-24.9 mm. The acromion marker of PP07 showed the largest error (37.2 mm), while for the other participants this error ranged from 10.5-13.8 mm.

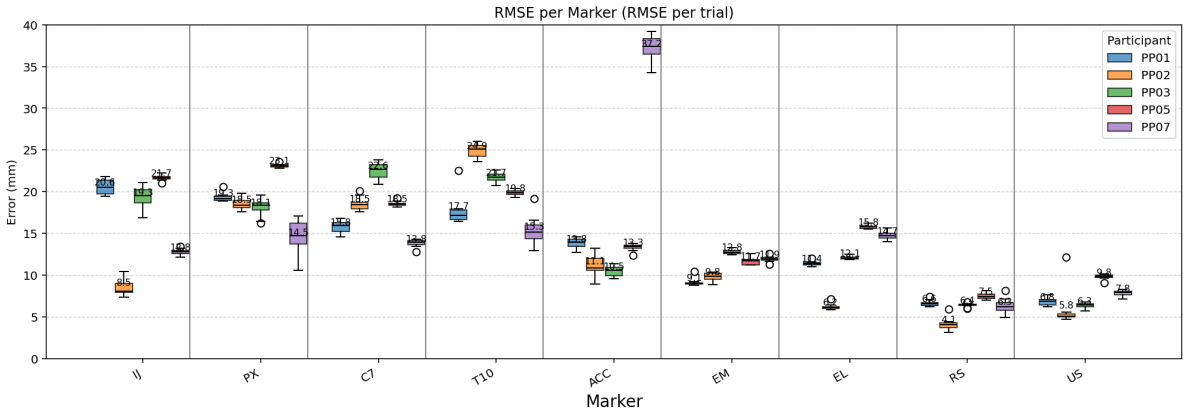

Figure 3.1: IK Marker Errors - grouped by participant

3.1.2. Inverse Dynamcs vs Static Optimization Work

Figure 3.2 illustrates the relative contribution of the reserve actuators from SO to the work of those actuators from ID over the whole motion. Values close to 0 indicate that the required joint moments were generated by the muscles, whereas values approaching 1 indicate a greater contribution from the reserve actuators. Since there are no muscles actuating the thorax and dominating the pronation/supination movement, those coordinates are not visualized in the plot. Additionally, the clavicular coordinates were excluded from interpretation due to the acromioclavicular constraint, which leads to non realistic torque, and therefore work, values.

The elbow flexion/extension exhibited the largest relative contribution from the reserve actuators with mean values ranging from approximately 50-83%. Also the axial rotation actuator showed relatively

high actuator contributions with mean values ranging from approximately 5-22%. All other shoulder coordinates demonstrated mean reserve actuator contributions below 5%, indicating that the muscles accounted for the majority of the moment generation required to reproduce the motion.

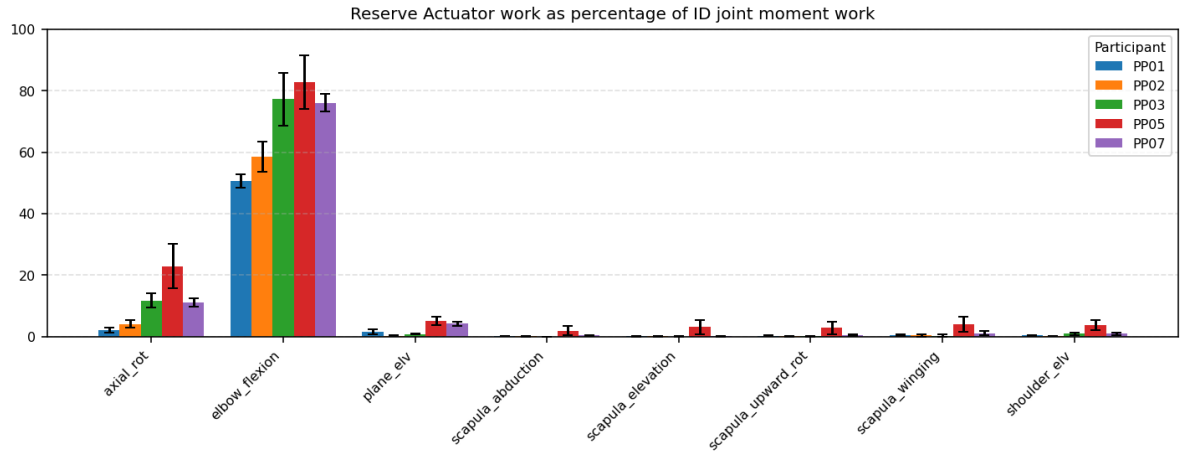

Figure 3.2: Percentage of absolute work of reserve actuators during SO relative to the work of the actuators done during ID - grouped by participant

Figure 3.3 summarizes the mean mechanical work of the thorax, the upper extremity (shoulder, elbow, pro-/supination) coordinate work during ID, and the main actuators across all participants for each of the three analysis windows active during SO. These windows represent: (1) the period from the trophy position to the thorax peak kinetic energy, (2) the interval from the thorax peak to the forearm peak kinetic energy, and (3) the final phase from the forearm peak to maximal internal rotation (MIR). This last window includes the moment of ball impact; see Appendix A for an illustration showing that ball impact occurs shortly after the forearm kinetic energy peak.

Across the first two windows, the total actuator work remains consistently low relative to systems energy. This indicates that during the early and middle phases of the serve, when kinetic energy is being progressively transferred along the kinetic chain, the model can largely resolve joint work through the musculature without substantial contributions from the reserve actuators.

In contrast, during the final window (from forearm peak to MIR), actuator work increases markedly for nearly all participants. This phase represents the deceleration phase of the serve and includes the time window of ball impact, during which high joint torques and rapid angular decelerations are present. The increased actuator contribution reflects the portion of coordinate work that could not be balanced by the muscles alone.

Among the actuators, the elbow actuators consistently exhibit the largest work values compared to the shoulder actuators (primarily axial rotation).

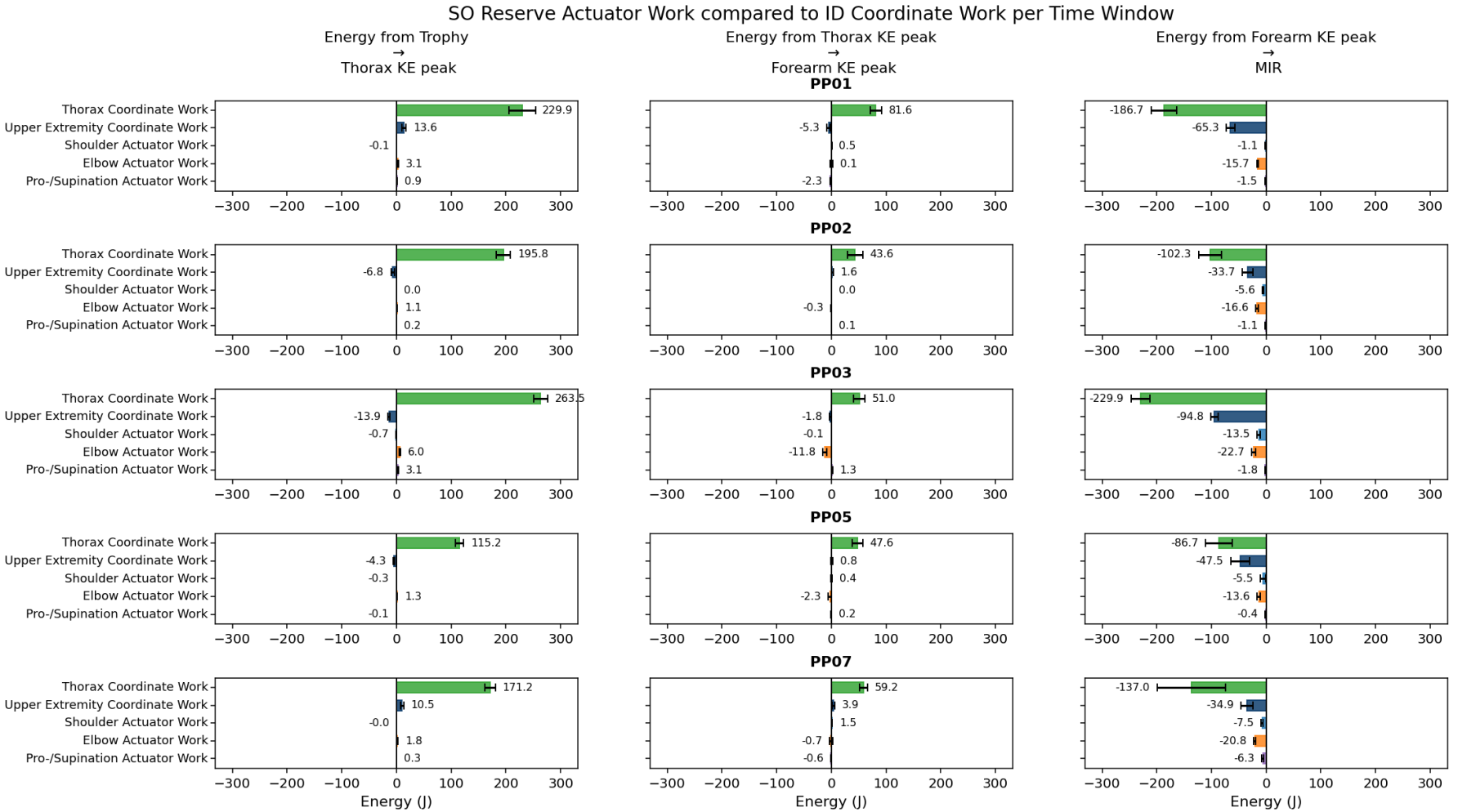

Figure 3.3: Percentage of absolute work of reserve actuators during SO relative to the work of the actuators done during ID per time window - grouped by participant

3.1.3. EMG Validation of Muscle Activations

Figure 3.4: Mean and ± SD of EMG and SO activations plotted per muscle per participant

The comparison between EMG signals and SO-predicted muscle activations showed participant-specific differences in correlation strength across all muscles (Table 3.1). Lag-corrected correlations ranged from weak to strong depending on both the muscle and the participant.

For the pectoralis major, both the clavicular and sternal portions showed moderate to strong correlations for most participants. The clavicular head showed strong correlations for PP01, PP03, PP05, and PP07, and a moderate correlation for PP02. Similarly, the sternal head showed strong correlations for PP01, PP03, PP05, and PP07, with PP02 showing a weak correlation.

The triceps brachii (long head) displayed strong or moderate correlations for PP01 and PP05, while PP02, PP03, and PP07 showed weak correlations. The latissimus dorsi showed moderate correlations for PP01, PP03, and PP05, and weak correlations for PP02 and PP07.

The deltoid (middle) showed more variation: PP03 exhibited a strong correlation, PP01 and PP05 moderate correlations, and PP02 and PP07 weak correlations. The biceps brachii (long head) showed moderate correlations for PP01 and PP05 and weak correlations for PP02, PP03, and PP07.

Overall, the correlations demonstrate variability across participants for all muscles, with the highest values observed for the pectoralis major and lower values more commonly observed for the biceps brachii and middle deltoid.

3.2. Energy Balance Across Time Windows

For each participant, three time windows were analysed: (1) from the trophy position to the thorax peak kinetic energy, (2) from thorax peak kinetic energy to the forearm peak kinetic energy, and (3) from forearm peak kinetic energy to maximum internal rotation (MIR). Within each window, net shoulder–elbow joint work (W_{ID}), reserve actuator work ($W_{\text{actuators}}$ for shoulder, elbow flexion and prosupination actuators) and the summed muscle work (W_{muscles}) were computed. Positive values indicate net energy generation, and negative values indicate net energy absorption.

PP01

In the trophy–thorax peak window, PP01 showed positive net shoulder+elbow joint work ($W_{\text{ID}} = +13.6$ J). Summed muscle work was $+9.4$ J and summed actuator work was $+4.0$ J. The largest positive muscle contributions in this phase were from SerratusAnterior ($+10.1$ J), Subscapularis ($+6.5$ J), and Tri-

Muscle	PP01	PP02	PP03	PP05	PP07
Biceps brachii (long head)	0.33±0.23	0.04±0.12	0.09±0.04	0.37±0.17	0.16±0.11
Triceps brachii (long head)	0.56±0.12	-0.15 ± 0.21	0.14±0.15	0.44±0.27	0.22±0.06
Deltoid middle	0.33±0.19	-0.12 ± 0.25	0.58±0.25	0.36±0.22	0.06±0.16
Pectoralis major (clavicular)	0.50±0.22	0.37±0.21	0.65±0.11	0.73±0.25	0.65±0.09
Pectoralis major (sternal)	0.68±0.28	0.18±0.22	0.71±0.18	0.70±0.10	0.63±0.06
Latissimus dorsi	0.47±0.13	0.14±0.12	0.34±0.26	0.48±0.19	0.11±0.01

Table 3.1: Lag-corrected EMG–SO correlations (mean ± SD) per participant and muscle. Cell shading indicates qualitative magnitude: Weak = Orange, Moderate = Yellow, Strong = Green.

ceps_Lat ($+5.4$ J), while the largest absorbing muscles were the Infraspinatus (-8.7 J), TrapeziusScapula_Upper (-1.9 J), and TeresMinor (-1.9 J).

In the thorax peak–forearm peak window, net joint work was slightly negative ($W_{\mathrm{ID}} = -4.4$ J), with summed muscle work of -4.1 J and summed actuator work of -1.4 J. The largest positive muscle work values were observed for SerratusAnterior ($+12.6$ J), Subscapularis ($+9.3$ J), and LevatorScapulae ($+2.6$ J), and the largest negative values for PectoralisMajorThorax (-14.2 J), BicepsBrevis (-6.0 J), and Infraspinatus (-3.7 J).

In the forearm peak–MIR window, net joint work was strongly negative ($W_{\mathrm{ID}} = -66.2$ J). Summed muscle work was -49.6 J and actuator work was -18.6 J. The muscles which generated most energy in this phase were SerratusAnterior ($+9.5$ J), TeresMajor ($+9.3$ J), and PectoralisMajorThorax ($+9.1$ J). The muscles contibuting most to the absorbtion of the energy are the LatissimusDorsi (-12.3 J), Deltoid_Medial (-11.9 J), and TrapeziusScapula_Lower (-11.4 J).

PP02

For PP02, the trophy–thorax peak window showed negative net shoulder+elbow joint work ($W_{\mathrm{ID}} = -6.8$ J). Summed muscle work was -4.5 J and actuator work $+1.3$ J. The largest positive muscle contributions were from SerratusAnterior ($+8.1$ J), Deltoid_Medial ($+5.6$ J), and Triceps_Med ($+4.3$ J), whereas the largest negative contributions came from Infraspinatus (-10.0 J), BicepsBrevis (-4.1 J), and Coracobrachialis (-3.6 J).

In the thorax peak–forearm peak window, net joint work was slightly positive ($W_{\mathrm{ID}} = +2.0$ J), with summed muscle work of $+2.6$ J and actuator work of $+0.4$ J. Deltoid_Medial ($+3.2$ J), SerratusAnterior ($+2.9$ J), and Infraspinatus ($+1.7$ J) showed the largest positive work values, while BicepsBrevis (-5.2 J), Coracobrachialis (-2.2 J), and BicepsLong (-0.6 J) displayed the largest negative work.

In the forearm peak–MIR window, net joint work was negative ($W_{\mathrm{ID}} = -34.1$ J), with summed muscle work of -8.9 J and actuator work of -23.9 J. The muscles generating most work had were the Deltoid_Posterior ($+5.5$ J), PectoralisMajorClavicle ($+5.0$ J), and PectoralisMajorThorax ($+4.3$ J) muscles, and the absorbing muscles were the TrapeziusScapula_Lower (-8.1 J), BicepsBrevis (-7.1 J), and BicepsLong (-4.4 J).

PP03

PP03 showed negative net joint work in the trophy-thorax peak window ($W_{\mathrm{ID}} = -13.9$ J). Summed muscle work was -20.6 J, while actuator work was $+8.4$ J. The muscles with the largest positive work were SerratusAnterior ($+12.6$ J), Triceps_Med ($+3.2$ J), and LevatorScapulae ($+1.8$ J). The largest negative values were observed in Infraspinatus (-7.2 J), TeresMinor (-5.5 J), and BicepsBrevis (-5.0 J).

In the thorax peak-forearm peak window, net joint work was close to zero but slightly negative ($W_{\text{ID}} = -1.3$ J). Summed muscle work was $+7.4$ J and actuator work was -9.8 J. The muscles with the largest positive work were SerratusAnterior ($+10.4$ J), Subscapularis ($+7.4$ J), and LevatorScapulae ($+2.7$ J), whereas the largest negative values were found for TrapeziusScapula_Lower (-8.9 J), TeresMinor (-3.0 J), and BicepsLong (-2.2 J).

In the forearm peak–MIR window, net shoulder+elbow joint work was strongly negative ($W_{\text{ID}} = -95.3$ J). Summed muscle work was -55.6 J and actuator work -38.9 J. The largest positive muscle contributions were SerratusAnterior ($+28.2$ J), PectoralisMajorClavicle ($+10.9$ J), and Subscapularis ($+8.9$ J). The main absorbing muscles were Deltoid_Medial (-27.0 J), Rhomboids (-24.7 J), and LatissimusDorsi (-14.4 J).

PP05

For PP05, the trophy–thorax peak window showed negative net joint work ($W_{\text{ID}} = -4.3$ J), with summed muscle work of -2.7 J and actuator work of $+0.9$ J. The main muscles delivering work were the SerratusAnterior ($+4.7$ J), Triceps_Lat ($+4.1$ J), and PectoralisMinor ($+2.0$ J). The muscles mainly absorbing the energy were the TeresMinor (-4.4 J), Infraspinatus (-4.3 J), and TrapeziusScapula_Upper (-2.3 J).

In the thorax peak–forearm peak window, net joint work was slightly positive ($W_{\text{ID}} = +1.1$ J). Summed muscle work was $+3.4$ J and actuator work -1.5 J. The muscles with the largest positive work values were SerratusAnterior ($+8.0$ J), Subscapularis ($+6.2$ J), and Triceps_Lat ($+3.8$ J). The largest negative values were observed for TeresMinor (-8.6 J), Infraspinatus (-8.1 J), and BicepsLong (-5.4 J).

In the forearm peak–MIR window, net joint work was negative ($W_{\text{ID}} = -47.8$ J), with summed muscle work of -23.7 J and actuator work of -19.8 J. The three largest positive muscle contributions were LevatorScapulae ($+11.1$ J), Rhomboids ($+6.9$ J), and PectoralisMajorThorax ($+5.5$ J). The largest negative values were found for TrapeziusScapula_Lower (-19.2 J), Deltoid_Medial (-15.9 J), and LatissimusDorsi (-9.7 J).

PP07

PP07 showed positive net joint work in the trophy–thorax peak window ($W_{\text{ID}} = +10.6$ J). Summed muscle work was $+9.1$ J and actuator work was $+2.0$ J. The largest positive muscle contributions were Deltoid_Medial ($+8.1$ J), SerratusAnterior ($+6.8$ J), and Coracobrachialis ($+5.0$ J), while the largest negative values came from Infraspinatus (-13.8 J), Rhomboids (-2.6 J), and LevatorScapulae (-2.2 J).

In the thorax peak–forearm peak window, net joint work remained positive ($W_{\text{ID}} = +3.8$ J). Summed muscle work was $+4.5$ J and actuator work $+0.4$ J. SerratusAnterior ($+12.4$ J), Subscapularis ($+4.3$ J), and PectoralisMajorThorax ($+4.3$ J) showed the largest positive work values, whereas Infraspinatus (-9.3 J), Rhomboids (-6.5 J), and BicepsLong (-3.9 J) showed the largest negative values.

In the forearm peak–MIR window, PP07 exhibited negative net joint work ($W_{\text{ID}} = -34.8$ J). Summed muscle work was -0.5 J, while actuator work was -34.7 J. The largest positive muscle work values in this phase were PectoralisMajorThorax ($+10.4$ J), SerratusAnterior ($+7.4$ J), and Subscapularis ($+4.9$ J). muscles absorbing most energy were the BicepsLong (-6.9 J), Deltoid_Medial (-6.5 J), and TrapeziusScapula_Lower (-5.4 J).

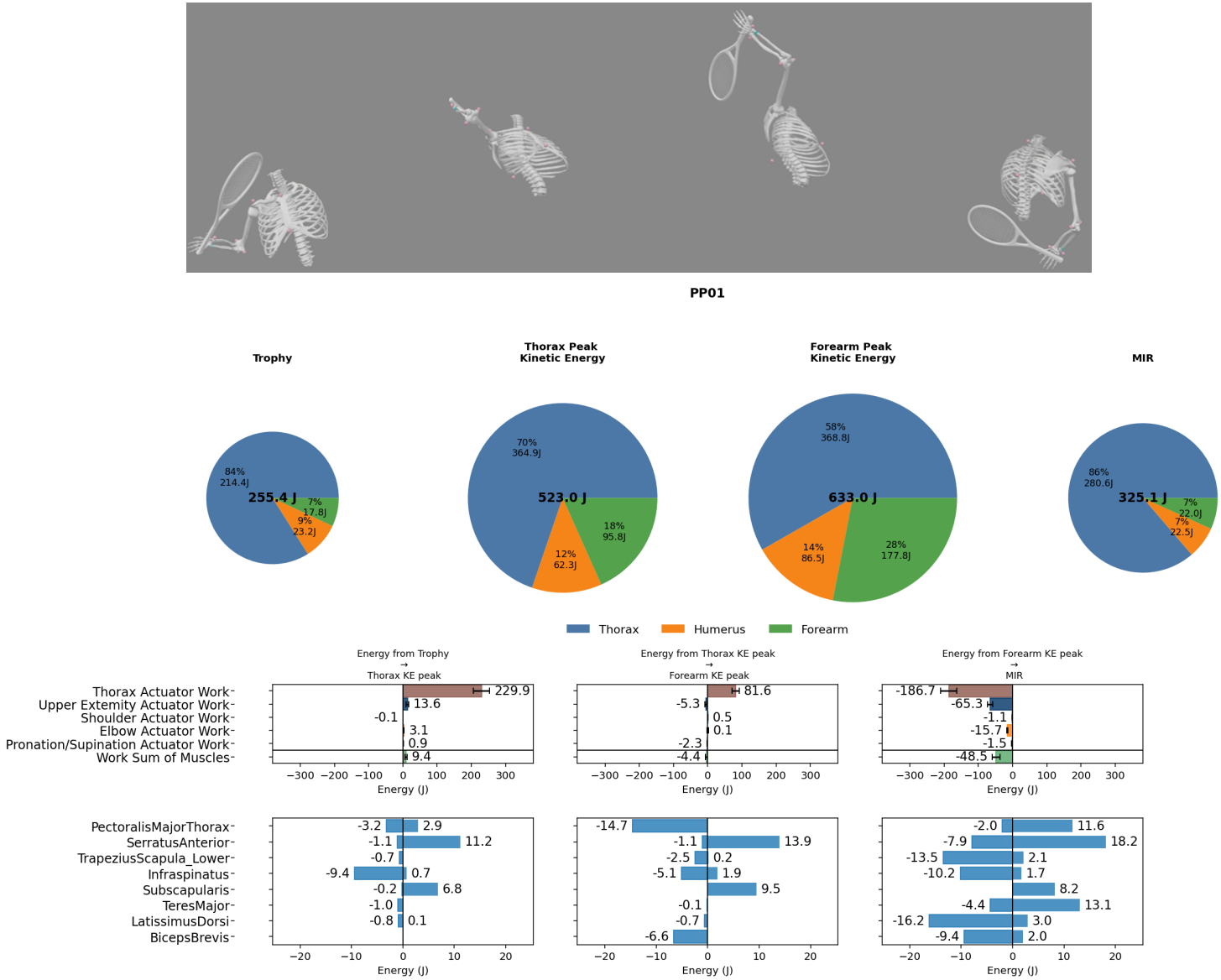

Figure 3.5: Overview of the energy state and muscle work for participant PP01 during the serve. (A) Pie charts show the instantaneous distribution of total system energy (kinetic + potential) at four timestamps: trophy position, thorax peak kinetic energy, forearm peak kinetic energy, and maximum internal rotation (MIR). (B) Net mechanical work performed by each actuator group between the selected timestamps. (C) Individual muscle work contributions over the same interval. Positive values indicate energy generation; negative values represent absorption.

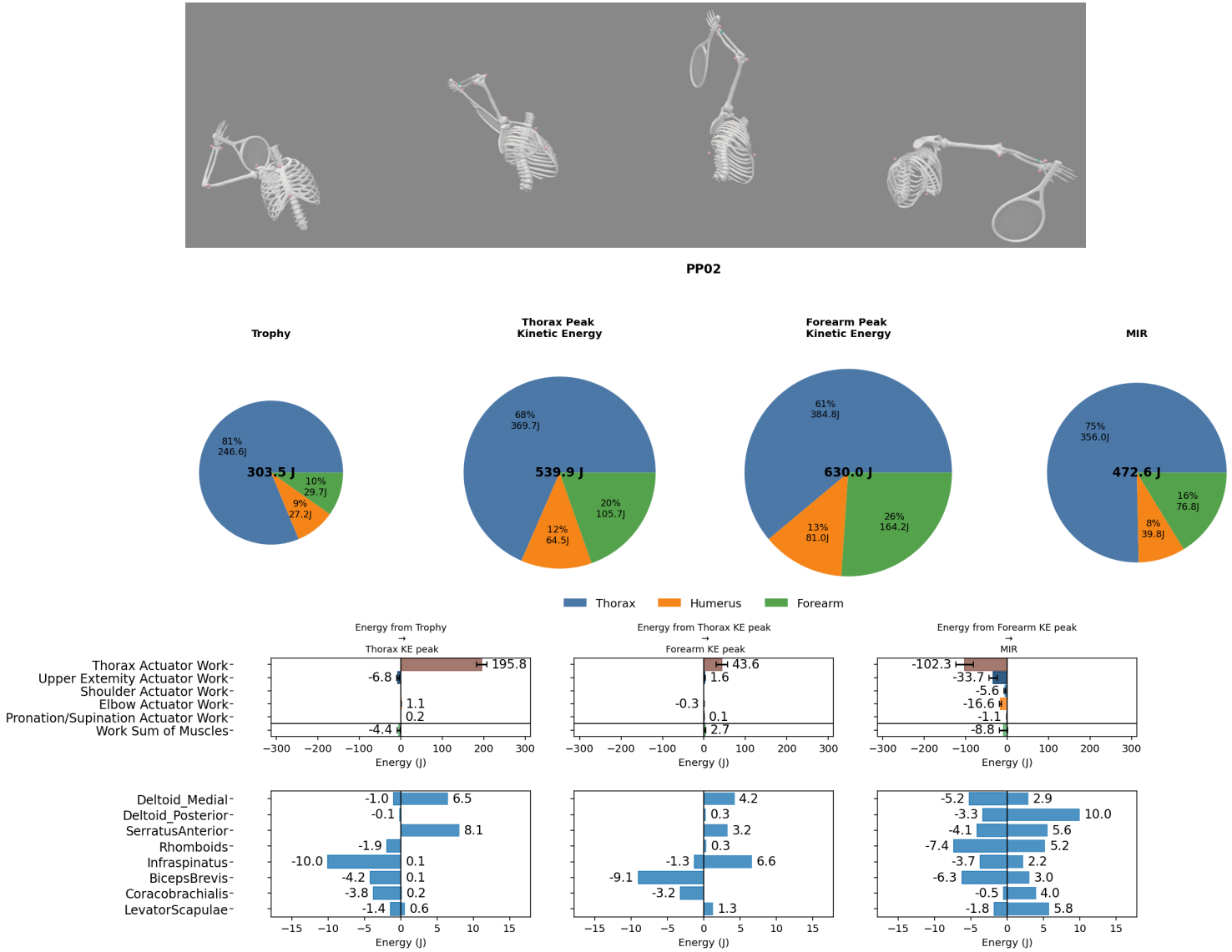

Figure 3.6: Overview of the energy state and muscle work for participant PP02 during the serve. (A) Pie charts show the instantaneous distribution of total system energy (kinetic + potential) at four timestamps: trophy position, thorax peak kinetic energy, forearm peak kinetic energy, and maximum internal rotation (MIR). (B) Net mechanical work performed by each actuator group between the selected timestamps. (C) Individual muscle work contributions over the same interval. Positive values indicate energy generation; negative values represent absorption.

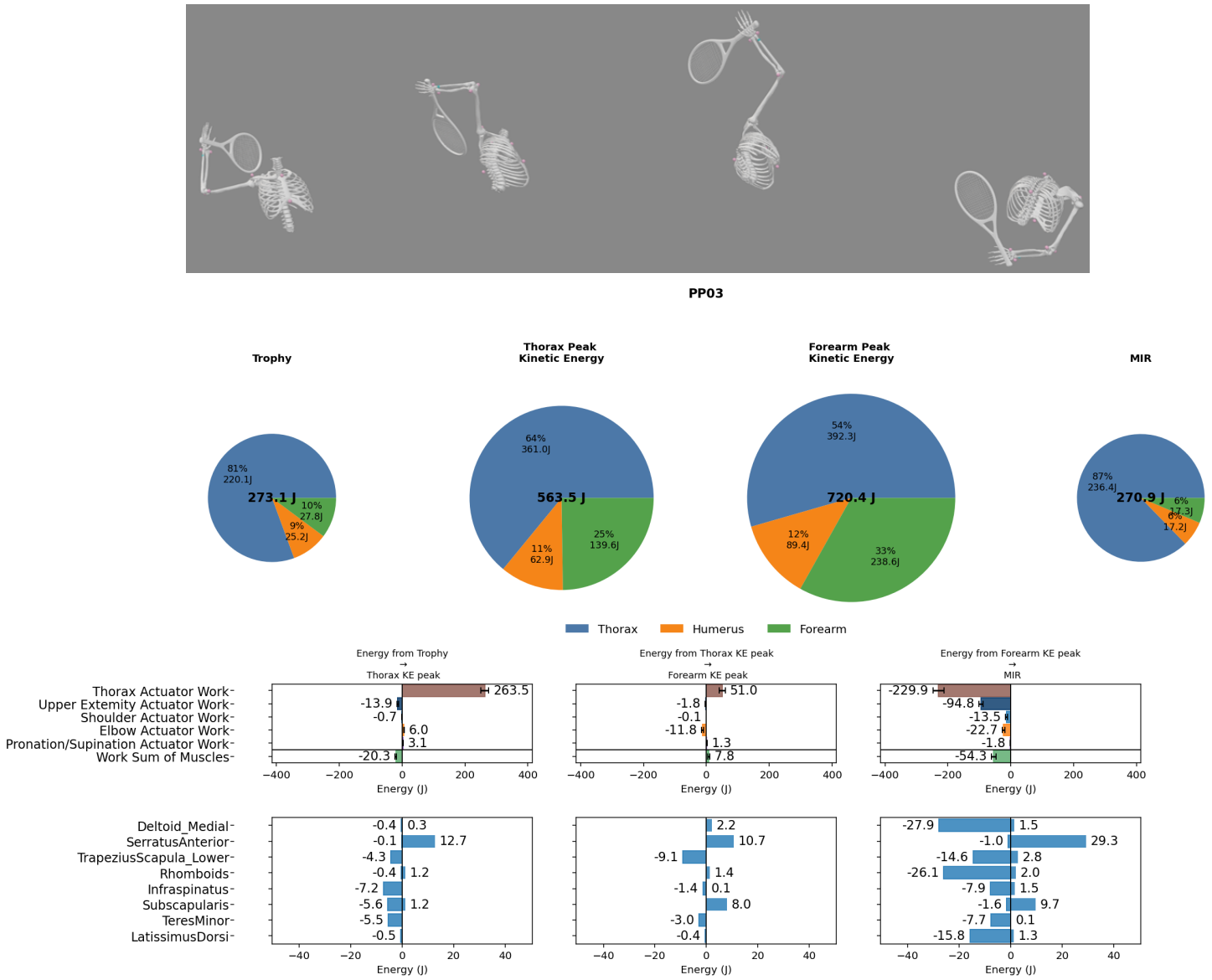

Figure 3.7: Overview of the energy state and muscle work for participant PP03 during the serve. (A) Pie charts show the instantaneous distribution of total system energy (kinetic + potential) at four timestamps: trophy position, thorax peak kinetic energy, forearm peak kinetic energy, and maximum internal rotation (MIR). (B) Net mechanical work performed by each actuator group between the selected timestamps. (C) Individual muscle work contributions over the same interval. Positive values indicate energy generation; negative values represent absorption.

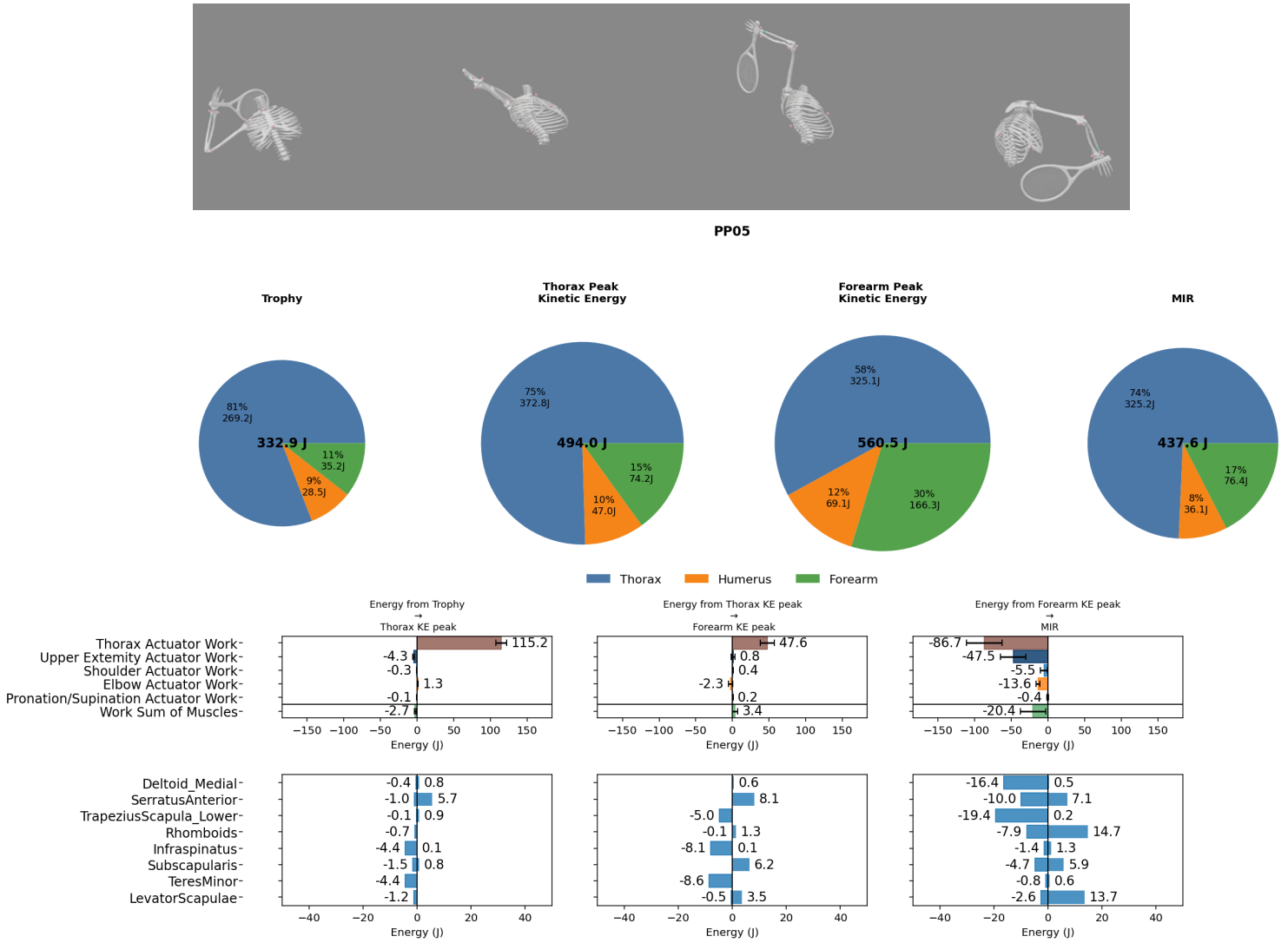

Figure 3.8: Overview of the energy state and muscle work for participant PP05 during the serve. (A) Pie charts show the instantaneous distribution of total system energy (kinetic + potential) at four timestamps: trophy position, thorax peak kinetic energy, forearm peak kinetic energy, and maximum internal rotation (MIR). (B) Net mechanical work performed by each actuator group between the selected timestamps. (C) Individual muscle work contributions over the same interval. Positive values indicate energy generation; negative values represent absorption.

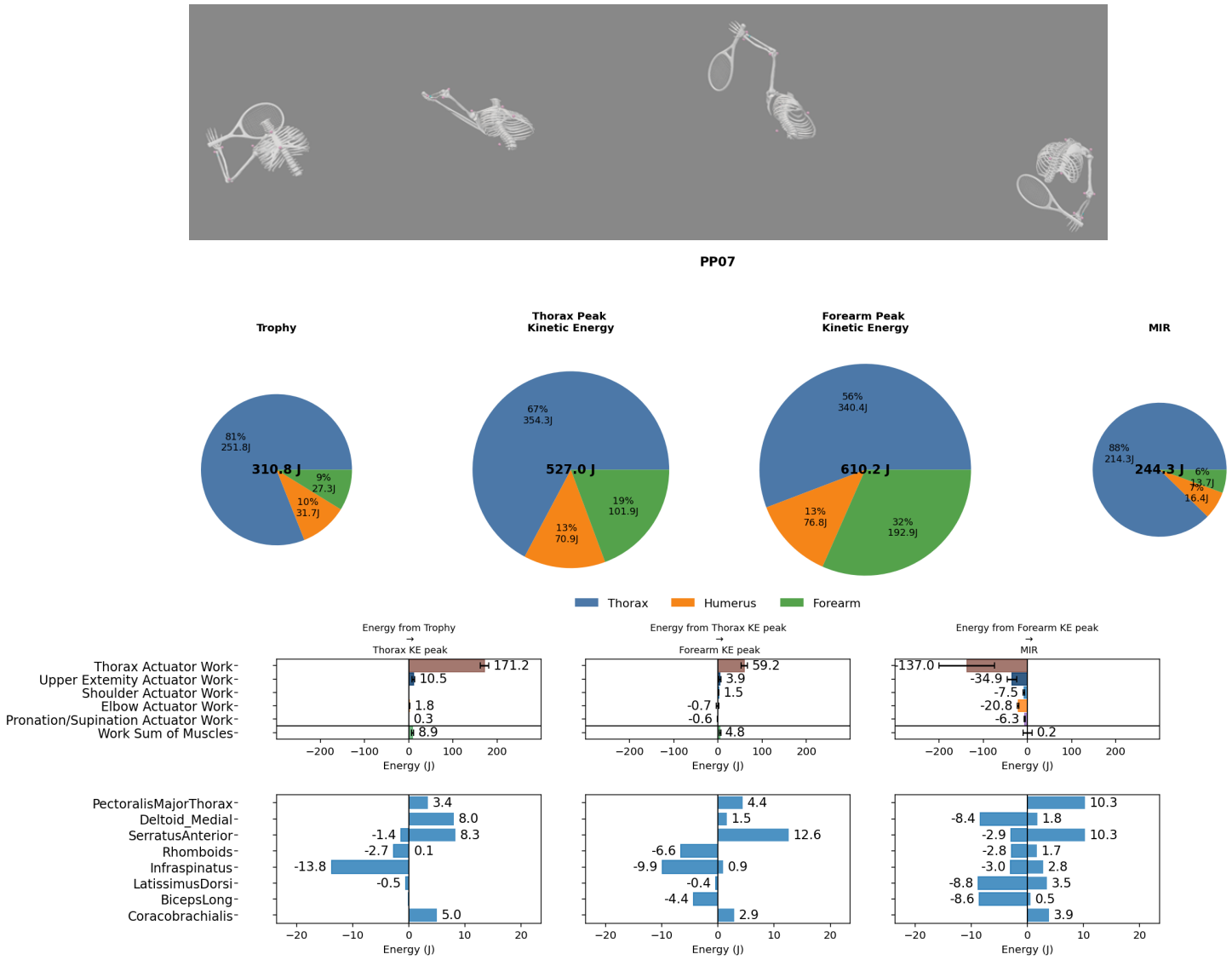

Figure 3.9: Overview of the energy state and muscle work for participant PP07 during the serve. (A) Pie charts show the instantaneous distribution of total system energy (kinetic + potential) at four timestamps: trophy position, thorax peak kinetic energy, forearm peak kinetic energy, and maximum internal rotation (MIR). (B) Net mechanical work performed by each actuator group between the selected timestamps. (C) Individual muscle work contributions over the same interval. Positive values indicate energy generation; negative values represent absorption.

4

Discussion

The aim of this study was to examine how mechanical energy is generated, transferred, and absorbed in the upper extremity during the tennis serve, with particular focus on the shoulder and elbow joint work and the contributions of individual muscle groups. Three key phases of the serve were analysed: (1) the interval from the trophy position to the thorax peak kinetic energy, (2) the period between thorax peak kinetic energy and forearm peak kinetic energy, and (3) the subsequent interval from forearm peak kinetic energy to maximum internal rotation (MIR). Examining these specific windows enabled a phase-based description of how energy is managed throughout the serve and how different muscle groups contribute to the acceleration and deceleration of the upper extremity. Across participants, clear patterns emerged in the timing and direction of energy changes, although the magnitude and distribution of muscle contributions differed considerably between individuals.

4.1. Phase-Specific Patterns of Energy Flow

4.1.1. Early Acceleration: Trophy to Thorax Peak

From the trophy position to thorax peak, total system energy increases substantially across participants. During this phase, the athlete pushes off the ground, and the energy generated by the legs, hips and trunk muscles raises both kinetic and potential energy of the system until the thorax reaches its peak. Energy from thorax peak subsequently flows through the humerus to the forearm, also increasing the energy of the distal segments.

Throughout this period, the work performed by the thorax actuators reflects this transferred energy from the proximal segments. Shoulder and elbow net actuator work remains almost negligible, indicating that the upper extremity's energy increase is driven predominantly by energy transmission rather than by active contributions from muscles accelerating the humerus or forearm.

All participants exhibited simultaneous positive and negative muscle work across different muscles, irrespective of whether the net joint work was positive (e.g., PP01, PP07) or negative (e.g., PP02, PP03, PP05). Muscles consistently producing positive work included the Serratus Anterior, Subscapularis, Medial Deltoid, and, to a lesser extent, the Pectoralis Major. In contrast, negative work was commonly observed in the Infraspinatus, Teres Minor, Rhomboids, and portions of the Trapezius. Although these muscles demonstrate measurable work output, their anatomical roles, the sign of the work, and the relatively small summed contributions indicate that they do not meaningfully increase segmental energy or directly drive the humerus or forearm forward. Instead, they appear to position the humerus and forearm to facilitate efficient energy transfer.

Despite relatively modest changes in net mechanical energy at the joint level, the substantial positive and negative muscle work observed throughout this phase indicates that muscles are engaged in shaping the movement trajectory and maintaining joint stability, rather than altering total system energy.

4.1.2. Mid Acceleration: Thorax Peak to Forearm Peak

The mid-acceleration phase spans the interval between thorax peak and forearm peak. At the beginning of this phase, thorax energy decreases, as the thorax is braking. According to the conservation of angular momentum, momentum stored in the thorax is transferred to the more distal segments, which, due to their lower mass, increase in angular velocity. This results in a rise in humerus and forearm energy, clearly visible in the pie charts.

Across participants, total system energy remains relatively stable compared to the other two time windows. Nonetheless, a slight overall increase persists, suggesting that the lower extremity may still be contributing energy through continued push-off.

For all participants, the work done by the upper extremity actuators is even smaller than in the early acceleration phase, despite the markedly altered energy distribution across segments. Once again, this highlights that the system relies primarily on energy transfer rather than active, muscle-driven acceleration of the upper extremity. As in the early acceleration phase, net joint work remains low, yet many of the same shoulder and elbow muscles continue to exhibit positive and negative work. This demonstrates that net joint work alone can mask substantial opposing muscle-level contributions.

Together, these results indicate that while individual shoulder muscles perform positive or negative work, their net contribution to the system's total energy is negligible. This suggests that the muscles primarily position the scapula and humerus relative to the thorax to guide the flow of energy from the trunk to the upper extremity. Consequently, the increase in humeral and forearm energy during this phase is not due to muscles actively accelerating these segments, but rather due to segmental positioning that conserves angular momentum.

4.1.3. Deceleration Phase: Forearm Peak to MIR

After the forearm reaches its energy peak, its energy decreases, as does the total system's energy. Ball impact also occurs within this phase, at or shortly after the moment the forearm reaches its peak energy (Appendix A). The energy transferred to the forearm and racket during the acceleration phases must now be absorbed. Because energy cannot flow further distally, the upper extremity must dissipate this energy locally and/or transfer it back proximally.

This pattern is visible in Figures 3.5–3.9. Although the thorax and/or lower extremity absorbs the largest portion of the energy, the upper extremity actuators are also significantly active in this phase, in contrast to the acceleration phases. The muscles around the shoulder and elbow absorb a substantial amount of energy, reflecting their role in decelerating the arm during the deceleration phase. With the medial deltoid, lower trapezius, latissimus dorsi, Rhomboids, and posterior cuff contributing to the largest negative values. These results show that the muscles responsible for deceleration were predominantly shoulder abductors, scapular muscles, and external rotators, consistent with previous studies measuring high EMG activation signals during these phases [3].

Although the posterior rotator cuff is typically described as the primary decelerator of the arm [20, 4], the present results show that the middle deltoid absorbed substantial amounts of energy during the deceleration phase. This is biomechanically plausible, as the middle deltoid plays a major role in controlling humeral elevation and providing compressive stability in the scapular plane. When the humerus remains elevated during follow-through, the middle deltoid must eccentrically regulate the downward and inward motion of the arm, resulting in considerable energy absorption. This suggests that deceleration demands may be distributed more broadly across the deltoid complex than traditionally described, with inter-individual differences in technique contributing to variation in muscle dominance.

In contrast, PP07 showed less muscle-driven absorption and more negative work coming from the actuators, suggesting a different coordination pattern where the shoulder and elbow muscles contributed less to slowing the arm down, and the model relied more on non-muscular components. This may be due to poor acromion marker tracking, which could have affected the estimated positions of the glenohumeral joint and scapula.

4.2. Muscle Coordination and Forces

The primary function of the shoulder muscles during the serve is to regulate segment orientation and maintain joint stability so that energy from the trunk can be transmitted effectively to the upper extremity. Rather than acting as major contributors to net mechanical work, these muscles coordinate the motion of the scapula and humerus to preserve the kinetic chain and guide angular momentum.

The scapular muscles demonstrated a stabilising pattern across participants. The Serratus Anterior frequently performed positive work, reflecting its role in protraction and upward rotation of the scapula, preventing winging and maintaining proximity to the thorax [6]. The Lower Trapezius and Rhomboids typically exhibited negative work, indicating eccentric control of protraction or upward rotation. Together, these muscles do not accelerate the humerus directly, but orient and stabilise the scapula to provide an optimal base for glenohumeral motion. This interpretation aligns with literature of scapular function in overhead athletes, where scapular positioning is essential for effective energy transfer and shoulder stability [6, 27].

The Deltoid and rotator cuff muscles acted together to control humeral motion and stabilise the glenohumeral joint. The Deltoid positions the humerus by controlling its elevation angle and plane of motion, while the rotator cuff provides compressive stability. Although the Subscapularis occasionally showed positive work and the posterior cuff negative work, the magnitudes were small compared to the net flow of energy, and shoulder actuator work peaked at only 1.8 J across participants. This suggests that their primary role was not to generate humeral rotation but to maintain glenohumeral position during the serve motion. This interpretation is consistent with the “compressor cuff” concept [6], where co-contraction stabilises the joint under multiplanar loading rather than producing large joint torques.

During late acceleration and early deceleration, several large muscles (i.e.,Pectoralis Major, Serratus Anterior, and Subscapularis) continued to show positive work. These findings align with previous EMG studies indicating that the Pectoralis Major contributes to horizontal adduction control and anterior stabilisation during late arm motion [3, 20], and that the Serratus Anterior maintains scapular upward rotation and posterior tilt during deceleration [6].

An additional explanation for the observed positive work in these muscles is the presence of electromechanical deactivation delays. Inspection of muscle power curves (Appendix A) shows that the Pectoralis Major, Serratus Anterior, and Subscapularis reach peak power shortly after the forearm energy peak and then decrease rapidly. Given that the interval between MER and MIR is 0.37 ± 0.26 s, and that OpenSim’s default activation dynamics include a 40 ms deactivation delay, part of the observed positive work likely reflects decreasing activation while muscles continue to produce force. As these large muscles fade out, braking muscles such as the Latissimus Dorsi, Rhomboids and the posterior cuff absorb energy to decelerate the arm.

4.3. Functional Interpretation

The serve can be interpreted as a sequence of three functional demands placed on the body: energy generation in the lower extremity and trunk, energy transfer through the shoulder, and energy absorption during deceleration. These functions are performed through coordinated interactions between muscles spanning the scapulothoracic and glenohumeral joints. The present results provide insight into how these muscles contribute to each functional role.

Energy generation during the early and mid acceleration phases did not arise from the shoulder complex. As shown in Section 4.1, the increase in total system energy over this interval originated almost entirely from trunk motion. The small but consistent positive work observed in the Serratus Anterior, Subscapularis, and Pectoralis Major therefore reflects their contribution to positioning and aligning the scapulothoracic and glenohumeral joints so that trunk and/or lower extremity generated angular momentum can be directed efficiently into humeral rotation.

Energy transfer was facilitated by the combined action of the scapular muscles and the rotator cuff. The Serratus Anterior and Trapezius regulated scapular upward rotation, posterior tilt, and protraction, providing a stable and appropriately oriented glenoid surface for humeral motion [6, 27]. Concurrently, the rotator cuff maintained glenohumeral compression, enabling angular momentum from the thorax to be transferred into humeral rotations. The substantial co-contraction and balanced positive and

negative work during mid acceleration indicate that these muscles contribute primarily to preserving joint alignment during rapid changes in segmental velocity, rather than increasing total system energy.

Energy absorption during the deceleration phase was the most mechanically demanding component of the serve and was reflected in the largest magnitudes of negative joint work. Several muscle groups contributed to dissipating this energy, including the Rhomboids and Lower Trapezius, the Latissimus Dorsi, and the Medial Deltoid. The distribution of negative work varied considerably between participants. PP02 and PP05 demonstrated a scapular-dominant deceleration strategy, with a large proportion of negative work absorbed by scapular stabilisers. PP07 relied more on shoulder abductors, particularly the Deltoid, whereas PP01 and PP03 exhibited a more distributed absorption across muscle groups. These findings suggest that athletes may rely on different strategies to decelerate the arm.

Although the present study does not establish causal links to injury mechanisms, the identified differences in deceleration strategies may have implications for shoulder loading. For example, reliance on scapular brakers for a large share of energy absorption may increase the mechanical demand on the scapulothoracic musculature, which has been associated with altered scapular control and scapular dyskinesis [9]. Conversely, insufficient contribution from the rotator cuff or overreliance on abductors during deceleration may increase anterior shear forces or superior translation at the glenohumeral joint, mechanisms implicated in SLAP lesions and anterior shoulder instability [5]. While no definitive conclusions can be drawn from the current data, the participant-specific variations observed here highlight the potential value of examining individual coordination strategies when interpreting shoulder loading in overhead athletes. Such differences may offer a useful framework for future studies linking musculoskeletal coordination patterns to joint loading and injury risk in the tennis serve.

4.4. Model Verification and Validation

To evaluate the reliability of the musculoskeletal model and associated pipeline, several verification and validation checks were performed.

Marker Tracking Accuracy

- **Thorax markers.** Some thorax markers showed errors greater than 20 mm. In the model, the thorax is treated as a rigid segment, whereas in reality it twists during the loading phase of the tennis serve. This mismatch between the model's rigid representation and the thorax's actual motion helps clarify why the errors were larger in this region and highlights that some degree of discrepancy is unavoidable
- **PP07 acromion cluster (ACC).** PP07 displayed a markedly high error at the ACC marker. In this participant, the cluster showed visible soft-tissue artifacts in the raw trajectories, which explains the elevated residual without indicating a computational issue in the IK solver. Because of these artifacts, the results for PP07 should be interpreted with caution.

Actuator Work Reserve actuators remained low for most coordinates. Two coordinates showed larger negative actuator work values: axial rotation of the shoulder and elbow flexion. In both cases, the increases were concentrated in the narrow time window surrounding ball impact.

These errors could at least partly be explained by the system's energy loss at ball impact, which is transferred to the ball and cannot be controlled by the muscles. Assuming that the actuator work fully compensates for this loss (excluding energy dissipated at the wrist), the kinetic energy of the ball can be estimated using

$$E = \tfrac{1}{2}mv^2,$$

with $m = 0.058$ kg. For typical serve ball velocities of 80–121 km/h, this corresponds to approximately 20–40 J of energy. Actuator work of a similar magnitude was observed around impact, making this explanation plausible. .

EMG–SO Comparison To assess physiological plausibility of the muscle forces, simulated muscle activations were compared with band-pass filtered EMG signals. While the general timing of activity was consistent across many muscles, several differences were observed.

In particular, some muscles showed reductions in SO activation around ball impact, whereas EMG signals did not show corresponding drops. Because SO computes the instantaneous force-sharing solution that satisfies joint moments at each time frame, it responds directly to abrupt changes in joint dynamics. In contrast, EMG reflects neural drive, which does not necessarily change instantaneously in the same manner. These differences could have reduced the correlation between EMG and SO.

Representation of Scapular Motion The model did not include explicit scapular kinematics. Because no scapula markers were available, scapular motion was not tracked directly but was instead determined indirectly through the shoulder-girdle joint definitions (e.g., the acromioclavicular constraint) and the weighting of the associated joint coordinates. This approach limits the representation of fully three-dimensional scapular behaviour during the serve. Consequently, muscles whose function depends strongly on scapular orientation (e.g., Serratus Anterior, upper and lower trapezius) may not reflect the exact mechanical conditions occurring in vivo. Although this is a simplification, reliable scapular marker tracking is not feasible in high-speed overhead motions due to soft-tissue artefacts. Therefore, constraining scapular motion through shoulder-girdle mechanics provides a practical and commonly used alternative in upper-limb modelling.[21]

4.5. Limitations

Several limitations should be considered when interpreting these findings. First, the wrist was implemented as a WeldJoint, and racket kinematics were not incorporated into the inverse kinematics solution. Although the mass and inertia of the racket were included, the resulting distribution of loading between the wrist and elbow remains uncertain. In addition, fixing the wrist and adding the racket's inertia, the hand–forearm segment makes the distal segment heavier and unable to move on its own. Because the whip-like motion of the serve depends on a light, freely moving distal segment, this setup likely changes how momentum is passed through the chain and may shift some of the loading toward the elbow or shoulder. For that reason, the joint loads presented here should be interpreted with caution, as the model cannot fully capture the natural wrist and racket motion that normally occurs during a serve.

Second, the wrapping surface of the Subscapularis was replaced with a via-point to prevent non-physiological muscle paths at high external rotation angles (> 90 degrees). The modified path was checked to ensure that the Subscapularis maintained a positive internal rotation moment arm. However, it was not validated against imaging-based or cadaveric reference data and therefore the magnitude of Subscapularis contributions during acceleration should be interpreted with caution.

Thrid, the musculoskeletal model was based on cadaveric anatomy and does not capture sport-specific adaptations in muscle architecture that may occur in trained tennis players, particularly at extreme ranges of motion. Therefore, the estimated muscle contributions should be interpreted as generalized rather than subject-specific.

Finally, the sample size was limited, and cross-participant comparisons were descriptive rather than statistical. Observed similarities and differences should therefore be interpreted qualitatively.

4.6. Future Work

Future work should address the methodological limitations outlined above in order to move from generalized to subject-specific interpretations. In particular, incorporating individual anatomical data, experimentally measured scapular motion/dimensions, and explicit wrist and racket modeling would enable more accurate estimation of how energy is transferred, generated and dissipated within each athlete. Developing subject-specific models may allow mechanical load patterns to be linked directly to technical characteristics such as trunk–arm coordination or scapular control strategies. In the long term, such approaches could support use in training environments, where individualized musculoskeletal models may help coaches and athletes identify inefficient or high-load movement patterns and guide targeted strength or technique interventions before injury symptoms develop.

5

Conclusion

5.1. Conclusion

The aim of this thesis was to investigate how mechanical energy is generated, transferred, and absorbed across the shoulder complex during the tennis serve, and to identify which muscle groups contribute most to acceleration and deceleration of the arm. An upper-extremity musculoskeletal model was combined with motion capture and EMG data from five competitive male tennis players. Joint work, muscle work, and actuator work were quantified across three time windows based on thorax and forearm kinetic energy peaks.

Energy Transfer Across the Kinetic Chain

Within the modelled segments, energy transfer from the trunk to the upper extremity followed a clear phase-dependent pattern. From the trophy position to forearm peak, changes in net shoulder–elbow joint work were modest, even though individual muscles generated and absorbed substantial amounts of energy. This indicates that during early and mid acceleration, energy originating from the trunk is transferred to the upper extremity, rather than being generated by the shoulder muscles themselves.

In the late phase, from forearm peak to maximum internal rotation (MIR), all participants showed large negative joint work at the shoulder and elbow, reflecting rapid deceleration of the arm and racket. Reserve actuator work remained small during the early and mid phases but increased around ball impact for shoulder axial rotation and elbow flexion, consistent with the energy loss to the ball and with limitations of the model near impact. Overall, the results indicate that energy generated in the legs, hips, and trunk and transmitted through the thorax supplies most of the upper-extremity energy, that the shoulder complex redirects this energy during acceleration and that the shoulder and elbow absorb much of it during deceleration.

Muscle Contributions to Acceleration and Deceleration

Across participants, the early and mid-acceleration phases (trophy to forearm peak) were characterised by concurrent positive and negative muscle work. Even though the absolute magnitudes were small, these patterns are informative because they illustrate how muscles contribute to positioning and joint control while proximally generated energy is transferred to the arm. The Serratus Anterior, Subscapularis, and Medial Deltoid consistently produced positive work, while the Infraspinatus, Teres Minor, Rhomboids, and Lower Trapezius absorbed energy.

The Subscapularis and posterior cuff behaved as part of a “compressor cuff,” generating compressive forces that stabilise the glenohumeral joint and counteract shear during fast axial rotation. Their role here is not to accelerate the arm, but to keep the humeral head centred in the glenoid so that momentum arriving from the trunk can be redirected effectively into humeral rotation.

The scapular muscles showed a similar coordinated role. The Serratus Anterior and Trapezius contributed to upward rotation, posterior tilt, and controlled protraction. These motions keep the glenoid

aligned with the humerus during rapid arm elevation and allow the arm to move freely through the wind-up.They also help maintain a favourable arm position as the serve progresses. Together, this creates a stable and mechanically base for transferring energy from the trunk into humerus.

During the deceleration phase (forearm peak to MIR), the largest magnitudes of negative joint work were observed. Energy absorption was shared between scapular movers, abductors, and horizontal abductors, with a smaller but still relevant contribution from the posterior rotator cuff. The Medial Deltoid and Lower Trapezius frequently emerged as major absorbers, suggesting that these muscles play an important role in controlling the downward and inward motion of the elevated arm and in stabilising the scapula as the arm slows.

Implications

Taken together, the findings show that deceleration demands in the tennis serve are not borne solely by the posterior rotator cuff, but are distributed across a wider set of muscle groups, including scapular muscles and shoulder abductors. Players who absorbed energy more broadly across these groups generally exhibited lower posterior cuff forces, particularly in the teres minor, whereas participants with less distributed absorption required higher cuff forces to stabilise the glenohumeral joint. This suggests that the way deceleration is coordinated influences the mechanical demands placed on the posterior cuff. While the present study cannot establish causal links to injury, these patterns provide a useful basis for future work examining how individual deceleration strategies relate to posterior cuff loading in overhead athletes.

The study also underscores the strengths and limitations of the current modelling approach. Musculoskeletal modelling made it possible to resolve net joint work into muscle-level contributions and to explore energy flow across phases of the serve. At the same time, the absence of ground reaction forces, simplified scapular and wrist representations, and reliance on cadaver-based anatomy constrain the precision of the estimated muscle loads.

Future work incorporating a wrist joint, racket kinematics and racket–ball interaction and external force measurements will be essential to refine these estimates and translate them into practical guidelines for performance optimisation and injury prevention in tennis.

References

[1] F Bruning. *Shoulder kinematics in relation to electromyographic activity of the M. pectoralis major during the tennis serve*.

[2] Scott L. Delp et al. “OpenSim: Open-Source Software to Create and Analyze Dynamic Simulations of Movement”. In: *IEEE Transactions on Biomedical Engineering* 54.11 (2007), pp. 1940–1950. DOI: 10.1109/TBME.2007.901024.

[3] Rafael F. Escamilla Jr. et al. *Shoulder Muscle Recruitment Patterns and Related Biomechanics during Upper Extremity Sports*. Tech. rep. 7. 2009, S69–590. URL: https://motusspt.com/wp-content/uploads/2023/02/Shoulder-Muscle-Recruitment-_-Biomechanics-UE-sports-2009.pdf?utm_source=chatgpt.com.

[4] Glenn S. Fleisig et al. “Kinetics of Baseball Pitching with Implications About Injury Mechanisms”. In: *The American Journal of Sports Medicine* 23.2 (Mar. 1995), pp. 233–239. DOI: 10.1177/036354659502300218. URL: https://doi.org/10.1177/036354659502300218.

[5] Lyle JMicheli. “Superior labrum from anterior to posterior (SLAP) lesions”. In: *Encyclopedia of Sports Medicine* (Jan. 2011). DOI: 10.4135/9781412961165.n506. URL: https://doi.org/10.4135/9781412961165.n506.

[6] W. Ben Kibler MD and Lexington Clinic Sports Medicine Center. “The role of the scapula in athletic shoulder function”. In: *The American Journal of Sports Medicine* 26.2 (1998), pp. 325–325. URL: https://upload.orthobullets.com/journalclub/free_pdf/9548131.pdf.

[7] KNLTB. *Groei in het tennis- en padelspeelveld van de KNLTB in 2024: een succesvolle strategie*. Feb. 2025. URL: https://www.knltb.nl/nieuws/2025/02/groei-in-het-tennis-en-padelspeelveld-van-de-knltb-in-2024-een-succesvolle-strategie/ (visited on 10/13/2025).

[8] M. Kovacs and T. Ellenbecker. “An 8-Stage Model for Evaluating the Tennis Serve”. In: *Sports Health: A Multidisciplinary Approach* 3.6 (2011), pp. 504–513. DOI: 10.1177/1941738111414175.

[9] Paula M. Ludewig and Jonathan F. Reynolds. “The association of scapular kinematics and glenohumeral joint pathologies”. In: *Journal of Orthopaedic and Sports Physical Therapy* 39.2 (Jan. 2009), pp. 90–104. DOI: 10.2519/jospt.2009.2808. URL: https://doi.org/10.2519/jospt.2009.2808.

[10] Joseph Manzi and Brittany et al. Dowling. “The Relationship Between Maximum Shoulder Horizontal Abduction and Peak Shoulder Kinetics in Professional Pitchers”. In: *Sports Health* (2023).

[11] Joseph Manzi, Matthew Fury, and Brittany et al. Dowling. “A Comparison of Throwing Arm Kinetics and Ball Velocity in Professional Baseball Pitchers with the Fastest Segment Velocities”. In: *Journal of Shoulder and Elbow Surgery* (2025).

[12] Joseph Manzi, Allen Nicholson, and Brittany et al. Dowling. “Relationships Between Throwing Mechanics and Shoulder Anterior Force in High School and Professional Baseball Pitchers”. In: *Shoulder & Elbow* (2022).

[13] Caroline Martin, Pierre Touzard, and Loïc Fourel. “The Use of Biomechanical Analysis to Help Reduce Serve-Related Injuries”. In: *Sports Medicine in Tennis* (2023).

[14] Caroline Martin et al. “Energy Flow Analysis During the Tennis Serve”. In: *American Journal of Sports Medicine* (2014).

[15] Caroline Martin et al. “Energy flow analysis during the tennis serve”. In: *The American Journal of Sports Medicine* 42.11 (Aug. 2014), pp. 2751–2760. DOI: 10.1177/0363546514547173. URL: https://doi.org/10.1177/0363546514547173.

[16] S. Mecheri et al. “The serve impact in tennis: First large-scale study of big Hawk-Eye data”. In: *Statistical Analysis and Data Mining: The ASA Data Science Journal* 9.5 (2016), pp. 310–325. DOI: 10.1002/sam.11316.

[17] Andreas Christos Panagiotopoulos and Ian Martyn Crowther. “Scapular Dyskinesia, the forgotten culprit of shoulder pain and how to rehabilitate”. In: *SICOT-J* 5 (Jan. 2019), p. 29. DOI: 10.1051/sicotj/2019029. URL: https://doi.org/10.1051/sicotj/2019029.

[18] Apoorva Rajagopal et al. “Full-Body Musculoskeletal Model for Muscle-Driven Simulation of Human Gait”. In: *IEEE Transactions on Biomedical Engineering* 63.10 (2016), pp. 2068–2079. DOI: 10.1109/TBME.2016.2586891.

[19] Katherine R. Saul et al. “Benchmarking of Dynamic Simulation Predictions in Two Software Platforms Using an Upper Limb Musculoskeletal Model”. In: *Computer Methods in Biomechanics and Biomedical Engineering* 18.13 (2015), pp. 1445–1458. DOI: 10.1080/10255842.2014.916698.

[20] Shane T. Seroyer et al. “The kinetic chain in overhand pitching: its potential role for performance enhancement and injury prevention”. In: *Sports Health A Multidisciplinary Approach* 2.2 (Mar. 2010), pp. 135–146. DOI: 10.1177/1941738110362656. URL: https://doi.org/10.1177/1941738110362656.

[21] Ajay Seth et al. “Muscle contributions to Upper-Extremity movement and work from a musculoskeletal model of the human shoulder”. In: *Frontiers in Neurorobotics* 13 (Nov. 2019), p. 90. DOI: 10.3389/fnbot.2019.00090. URL: https://doi.org/10.3389/fnbot.2019.00090.

[22] Ajay Seth et al. “OpenSim: a musculoskeletal modeling and simulation framework for in silico investigations and exchange”. In: *Procedia IUTAM* 2 (2011), pp. 212–232. DOI: 10.1016/j.piutam.2011.04.021. URL: https://doi.org/10.1016/j.piutam.2011.04.021.

[23] Ajay Seth et al. “OpenSim: Simulating musculoskeletal dynamics and neuromuscular control to study human and animal movement”. In: *PLoS Computational Biology* 14.7 (2018), e1006223. DOI: 10.1371/journal.pcbi.1006223.

[24] Bart van Trigt. “Blessurepreventie bij bovenhandse sporten: Kunnen sensoren hierbij helpen?” In: *Sportgericht* (2024).

[25] Bart van Trigt, Marco Hoozemans, and Natasja van der Boon. “Hoe het hele lichaam bijdraagt aan de ‘ideale’ tennisslag”. In: *Sportgericht* (2025).

[26] Bart van Trigt et al. “Uncovering the Hidden Mechanics of Upper Body Rotations in Tennis Serves Using Wearable Sensors”. In: *Frontiers in Sports and Active Living* (2025).

[27] H. Van Der Hoeven and W. B. Kibler. “Shoulder injuries in tennis players”. In: *British Journal of Sports Medicine* 40.5 (2006), pp. 435–440. DOI: 10.1136/bjsm.2005.023218.

[28] Kevin E. Wilk et al. “Shoulder injuries in the overhead athlete”. In: *Journal of Orthopaedic and Sports Physical Therapy* 39.2 (Feb. 2009), pp. 38–54. DOI: 10.2519/jospt.2009.2929. URL: https://doi.org/10.2519/jospt.2009.2929.

[29] Toshimasa Yanai, Ryan Crotin, and Tanghuizi Du. “Proximal-to-Distal Sequencing Impacts on Maximum Shoulder Joint Angles and the Risk of Impingement in Baseball Pitching”. In: *Scandinavian Journal of Medicine & Science in Sports* (2023).

A

Energy & Muscle Power Plots

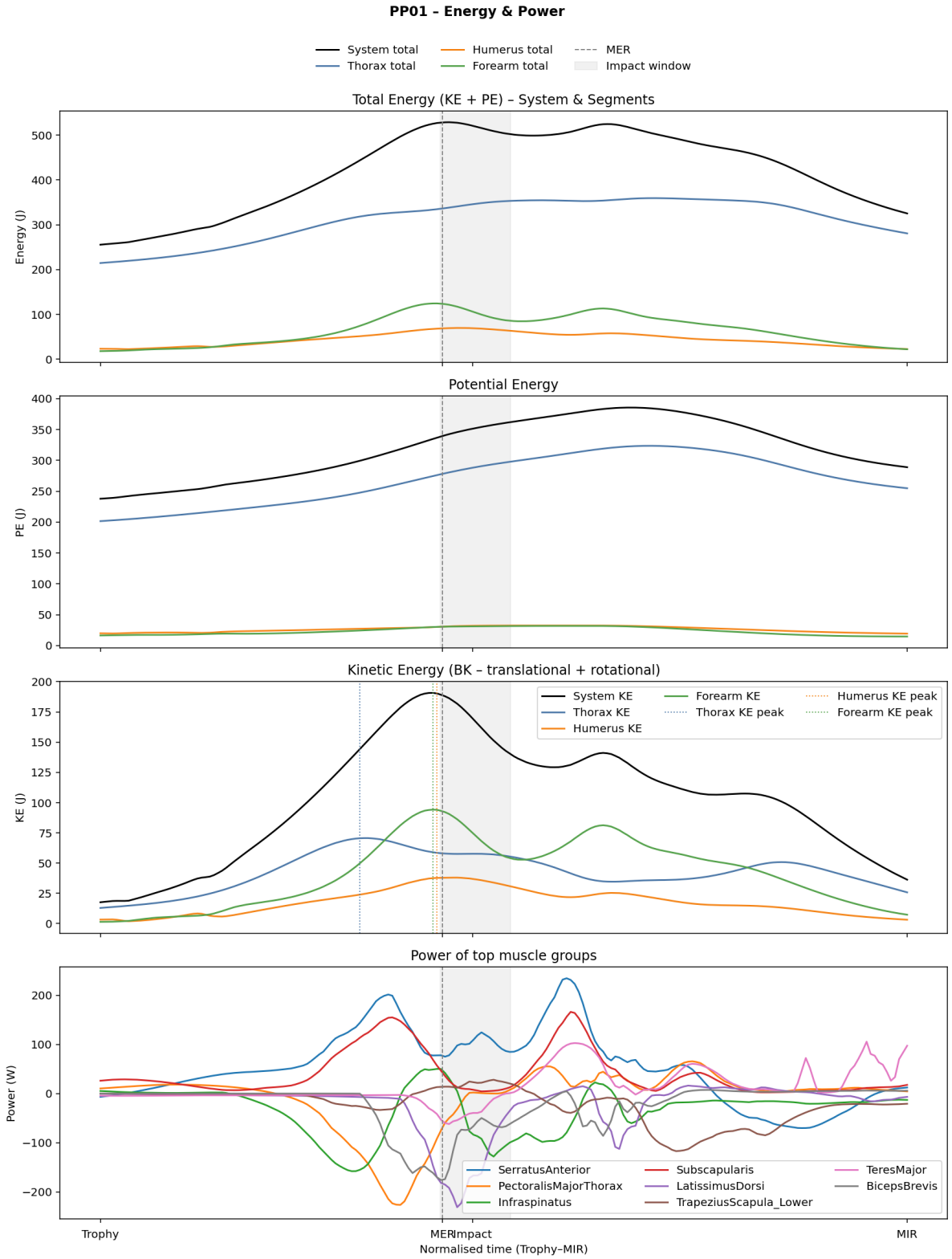

Figure A.1: PP01 Energy and Muscle Power over Time

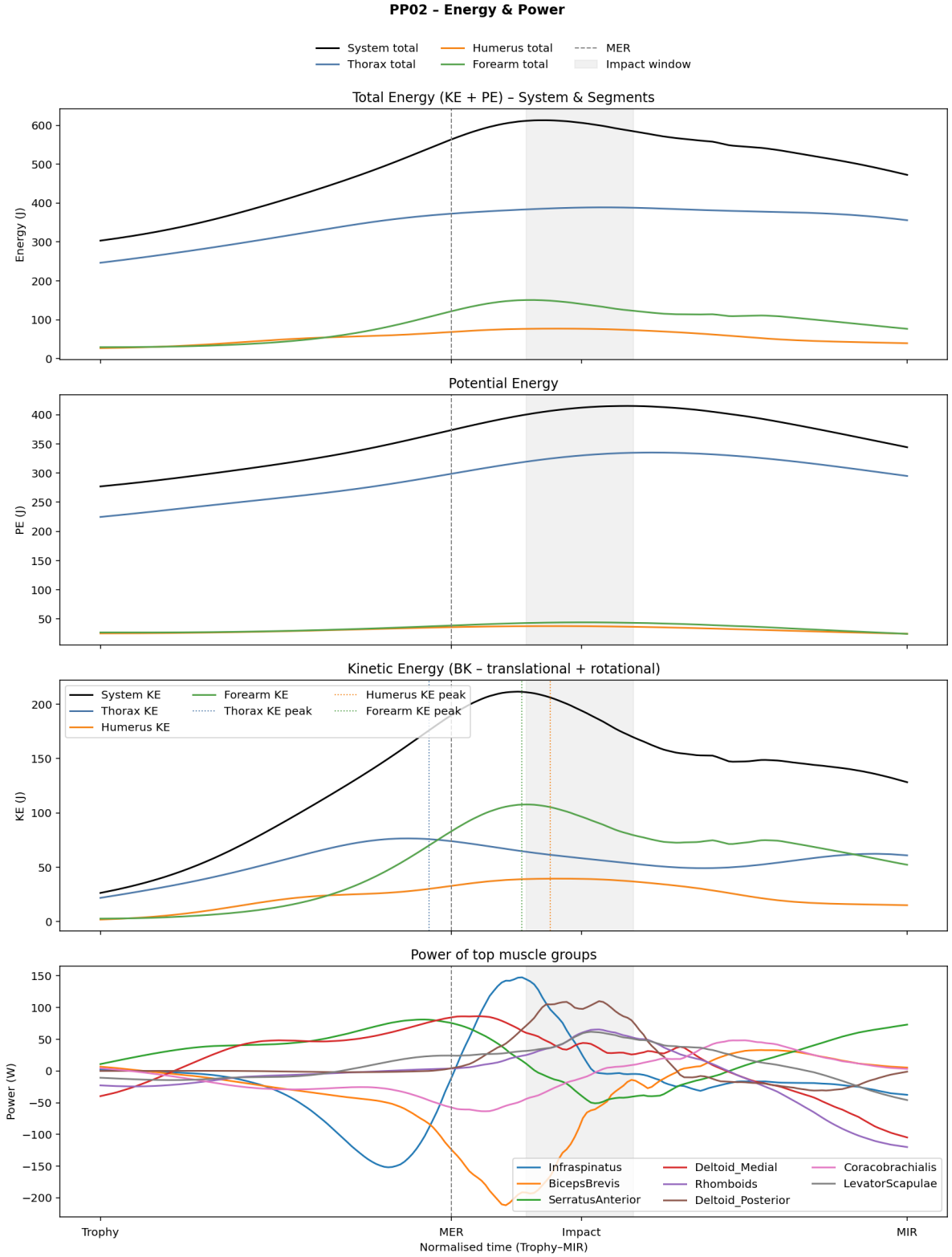

Figure A.2: PP02 Energy and Muscle Power over Time

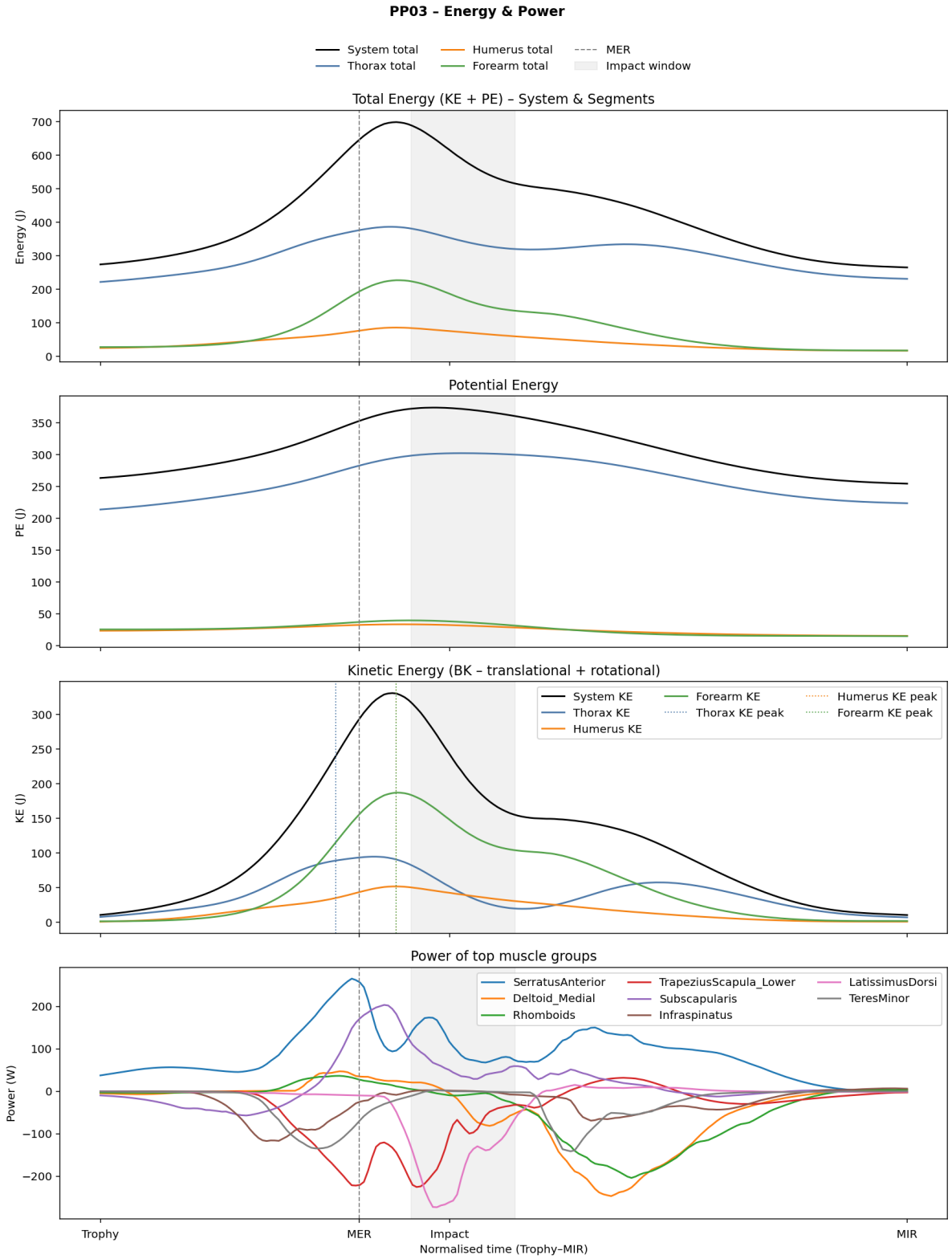

Figure A.3: PP03 Energy and Muscle Power over Time

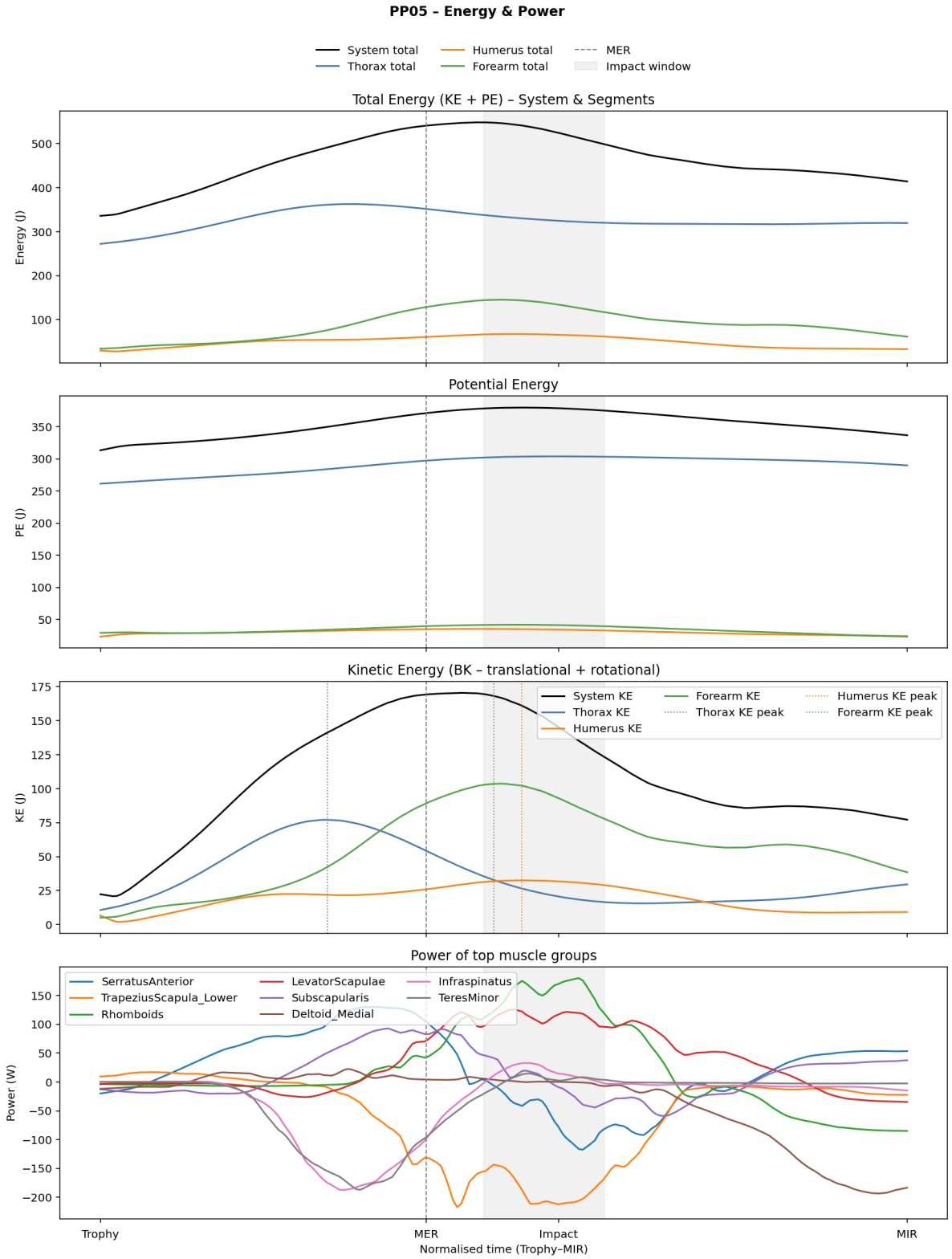

Figure A.4: PP05 Energy and Muscle Power over Time

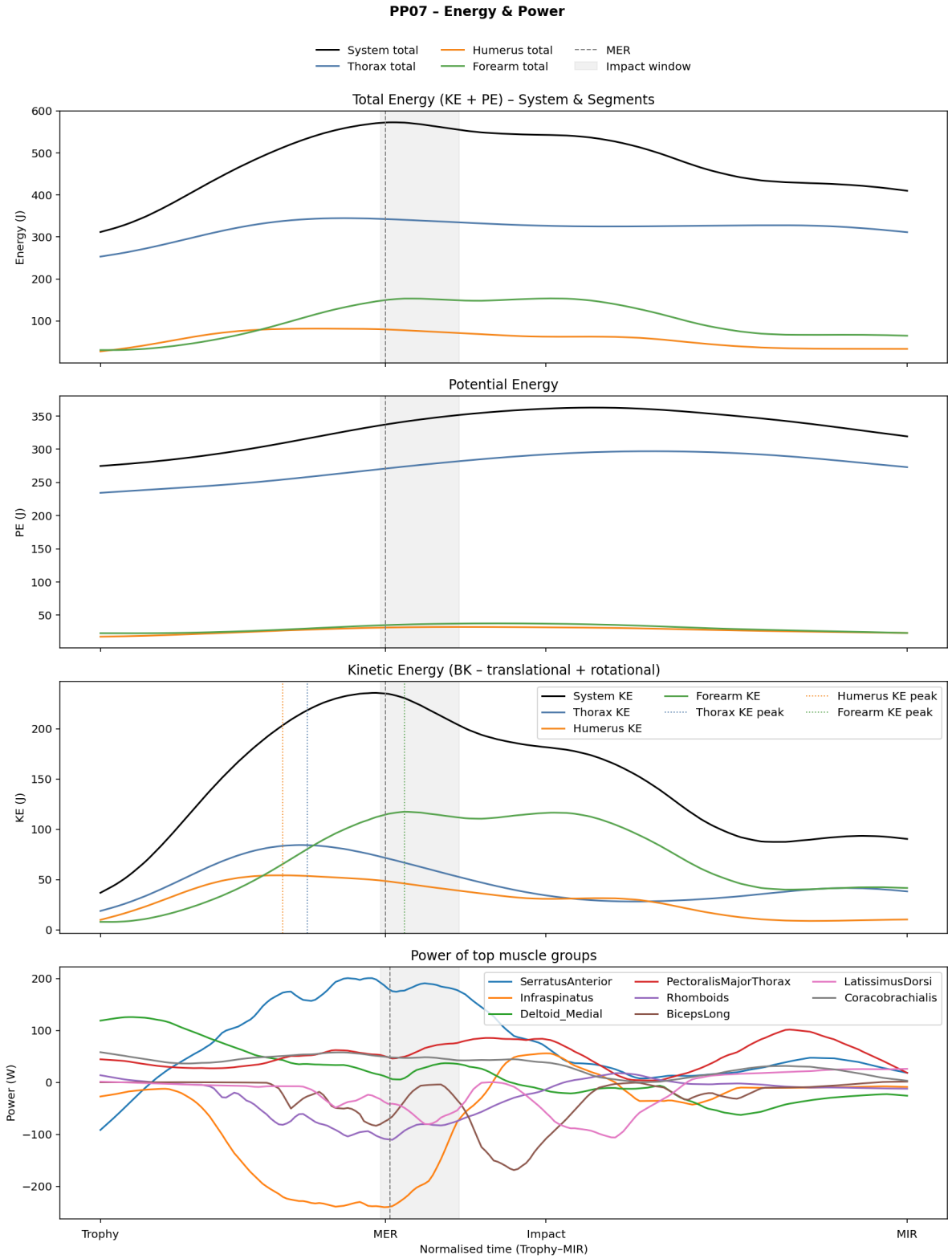

Figure A.5: PP07 Energy and Muscle Power over Time

B

Muscle Force Plots

PP01 – top 8 muscle groups (force vs time)

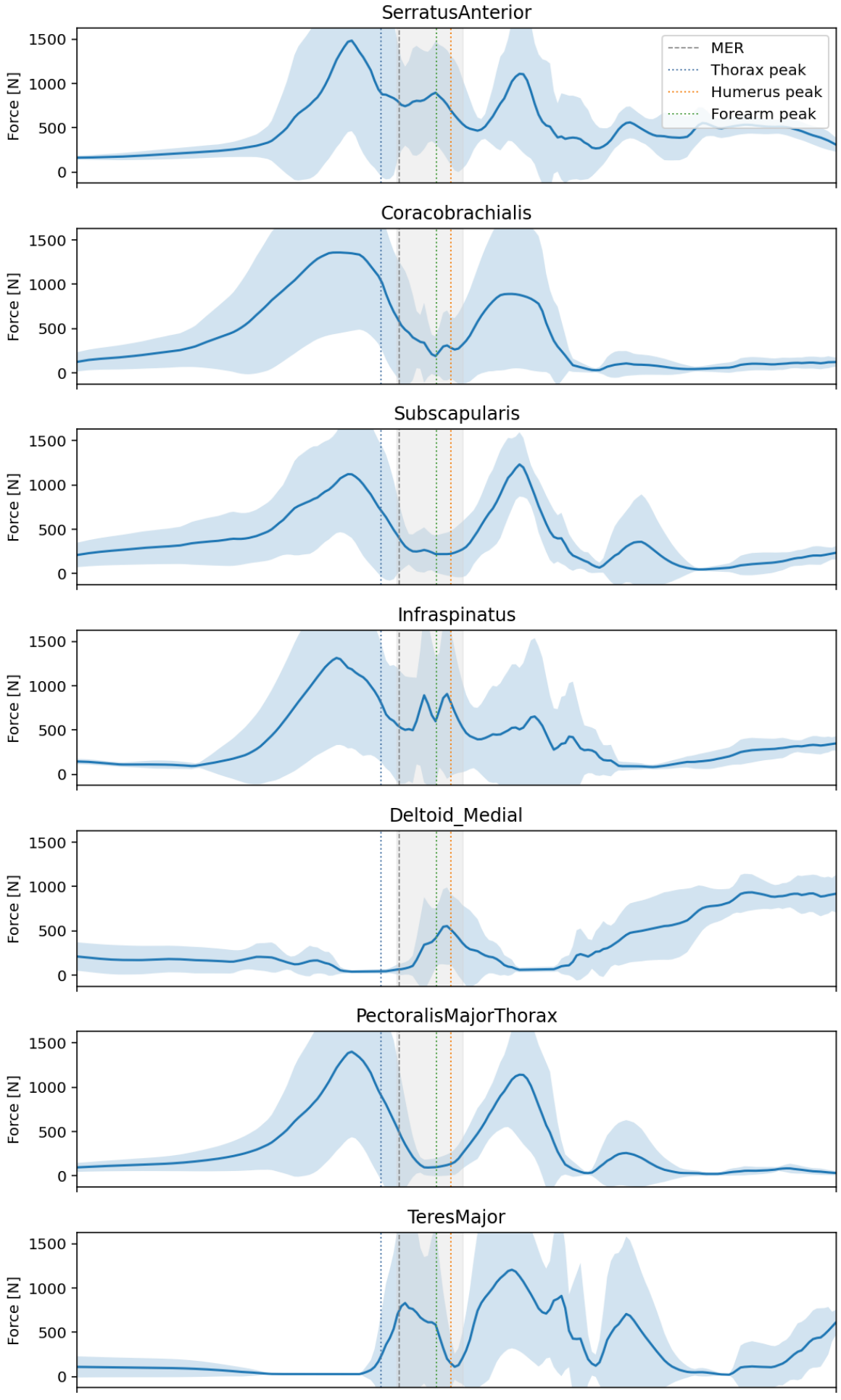

PP02 – top 8 muscle groups (force vs time)

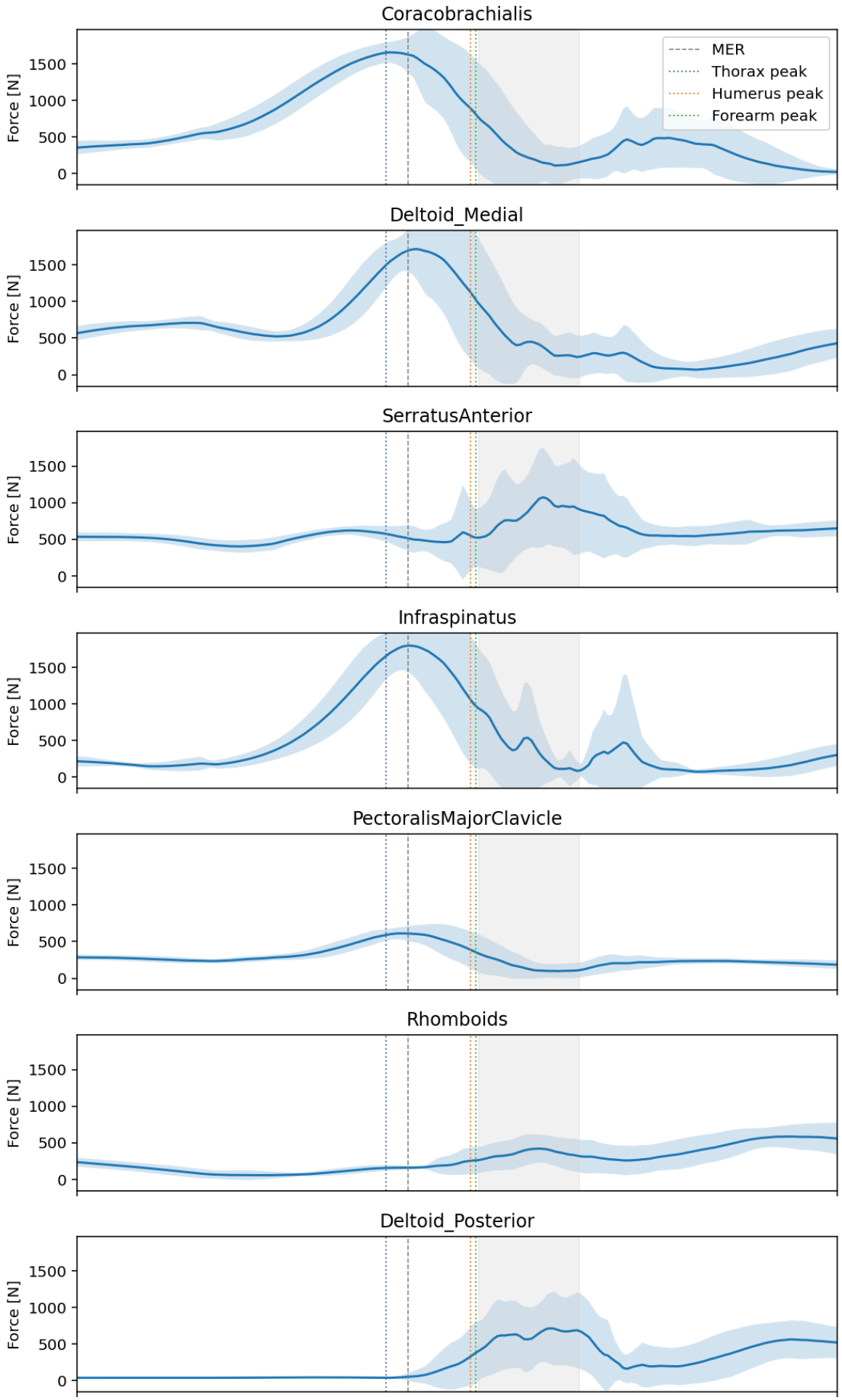

PP03 – top 8 muscle groups (force vs time)

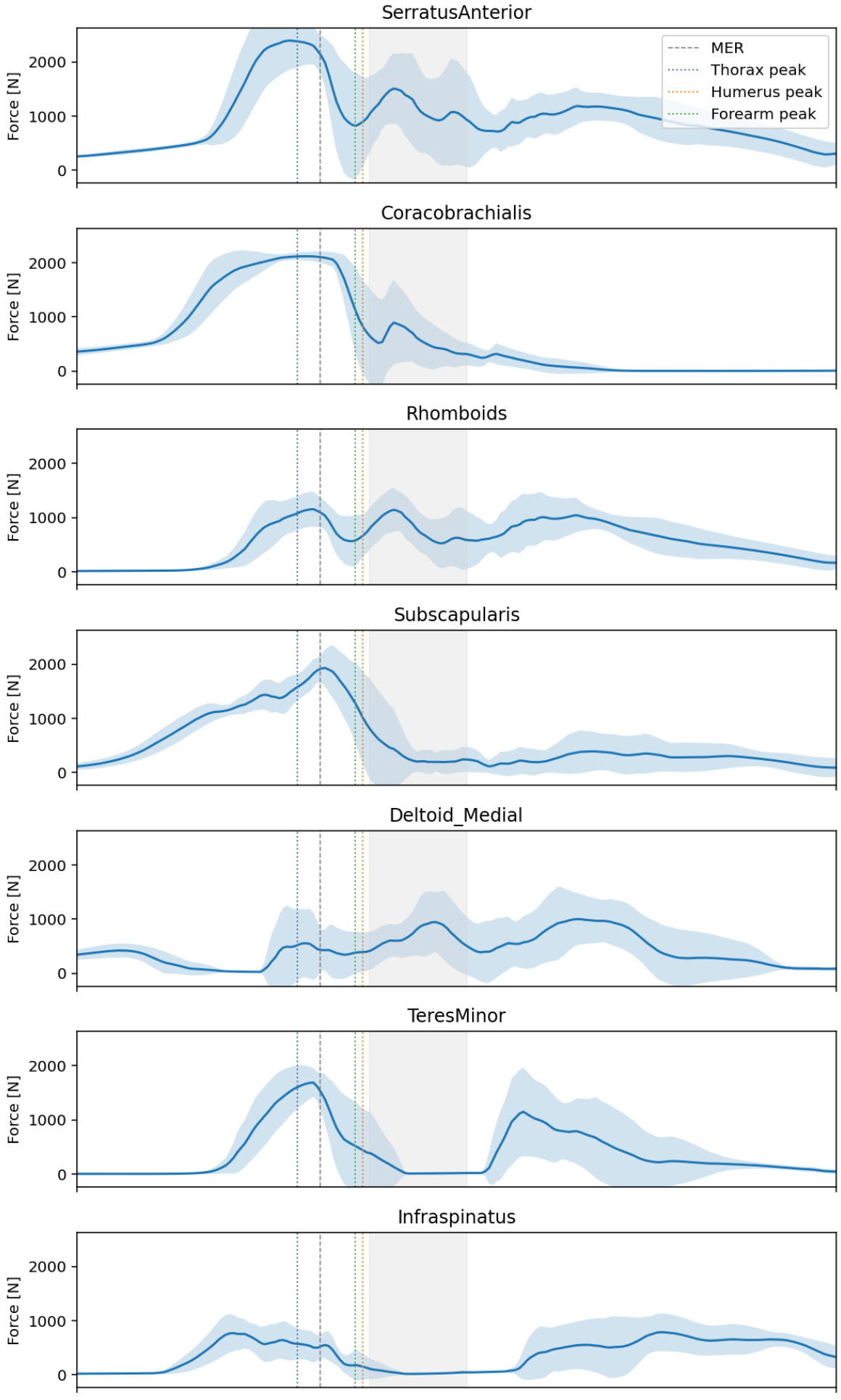

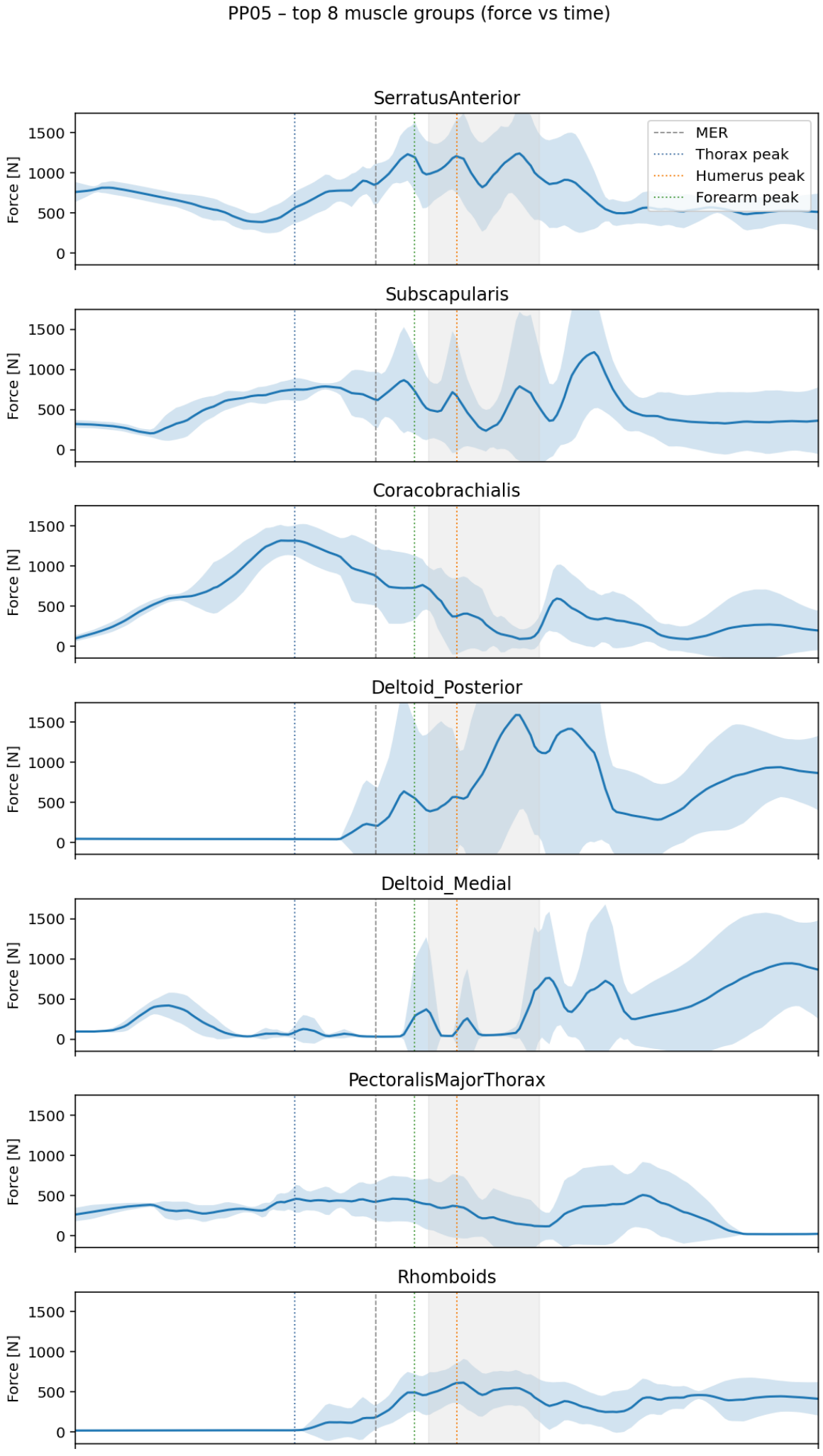
PP05 – top 8 muscle groups (force vs time)
SerratusAnterior
Subscapularis
Coracobrachialis
Deltoid_Posterior
Deltoid_Medial
PectoralisMajorThorax
Rhomboids
Force [N]
0
500
1000
1500
MER
Thorax peak
Humerus peak
Forearm peak

PP07 – top 8 muscle groups (force vs time)